NASA CR-
144395

SPACE SHUTTLE ORBITER
MECHANICAL REFRIGERATION SYSTEM

Contract No. NAS9-12055
Report No. T122-RP-038

FINAL REPORT

14 October 1974

Submitted By

VOUGHT SYSTEMS DIVISION
LTV Aerospace Corporation
Dallas, Texas

To

THE NATIONAL AERONAUTICS AND SPACE ADMINISTRATION
Johnson Space Center
Houston, Texas

FOREWORD

This is the Final Report on Contract NAS9-12055 which was executed by Vought Systems Division between January 1972 and October 1974. This is a Summary Report; the information contained in this report has been previously presented in detail in Progress Reports, and in two technical papers which are included as Appendices to this report.

The NASA-JSC technical monitors on this program were Mr. D. W. Morris on the system demonstration phase, and Mr. Burrell French on the zero-g condensation experiment phase.

TABLE OF CONTENTS

APPENDICES

LIST OF FIGURES

LIST OF TABLES

1.0 INTRODUCTION AND SUMMARY

In 1970 and 1971 Vought Systems Division (VSD) performed a study on use of refrigeration in rejection of future spacecraft environmental control system heat loads, under NASA-JSC contract NAS9-9912. One conclusion of that study was that vapor compression was the most attractive mechanical refrigeration concept for use in future spacecraft (Reference [1]). A revolutionary heat rejection system of a hybrid type was recommended for further study (Reference [2]). This was a hybrid refrigeration/radiator system which acts as either a refrigeration system or as a radiator system, depending on the vehicle heat rejection demand and the external environment. The hybrid system uses a common flow network and radiator condenser; compressors and pumps are valved into and from the flow loop as required. This system is particularly well suited to lunar surface shelters. Peak heat rejection requirements during the long lunar day coincide with peak power availability from solar cells; during the lunar night while power is scarce, the relatively efficient radiator mode is used.

There were several technical questions relating to the feasibility of this hybrid concept, including:

(1) Could the system be changed from the single-phase "radiator" mode of operation to the two-phase "refrigeration" mode?

(2) Could a radiator/condenser design be evolved which would provide satisfactory operation in both the "radiator" and the "refrigeration" modes of operation while in a zero-g field?

(3) Could a highly efficient motor-compressor unit capable of operation in a zero-gravity field be obtained?

The first of these questions was quickly answered in a feasibility demonstration test (Reference [3]), where it was shown that a hybrid system could be switched from one operating mode to the other without damage to system components.

NASA-JSC then contracted with VSD (in the subject contract) to design a suitable radiator/condenser and to demonstrate it in a thermal-vacuum test in a systems test. Later this contract was modified to include design, fabrication and ground checkout of an experiment apparatus which would verify the condenser flow design under simulated zero-g conditions.

This report briefly describes the design, fabrication and testing which were accomplished under contract NAS9-12055.

2.0 DISCUSSION

2.1 Systems Test

The purpose of the systems test was to demonstrate that a radiator/condenser could be designed which was efficient in both condensation ("refrigeration") and liquid phase ("radiator") operating modes. In addition, switchover from the "refrigeration" mode to the "radiator" mode and vice versa was to be demonstrated.

The major issues associated with design of the radiator/condenser were:

(1) tube layout

and (2) tube diameter

There was a desire to use the wide heat load range radiator concept (References [4], [5], and [6]) which has tubes of varying length as shown in Figure 1. In a liquid phase radiator this approach provides a heat load ratio of 100 to 1 or more, which is a distinct advantage in a spacecraft heat rejection system. However, it was found that the unequal flow lengths of the wide heat load radiator were unsuitable for a condensing radiator. There were two primary reasons for this:

(1) Orificing required in the wide heat load radiator tubes is difficult to size so that proper flowrates are established in both liquid and vapor flow.

(2) The wide heat load radiator has inherently higher pressure drop than a conventional parallel flow radiator, and this degrades performance in the two-phase or "refrigeration" mode of operation.

It was found that suitable performance could be obtained in both "radiator" and "refrigeration" modes of operation with tubes of 3.175 mm (1/8-in) inside diameter. This diameter tube, with the appropriate flowrates in each operating mode, produces acceptable pressure drop and heat transfer rates. In addition, it also promised flow stability in the condensing mode of operation in zero-gravity. In order to accomplish the design of the condensing radiator it was necessary to predict the pressure drop of a condensing two-phase flow in zero-gravity. A method for doing this was developed, based on the Lockhart-Martinelli approach (References [7] and [8]). The method developed is discussed in detail in Reference [9] and in Appendix A. It was also necessary to predict

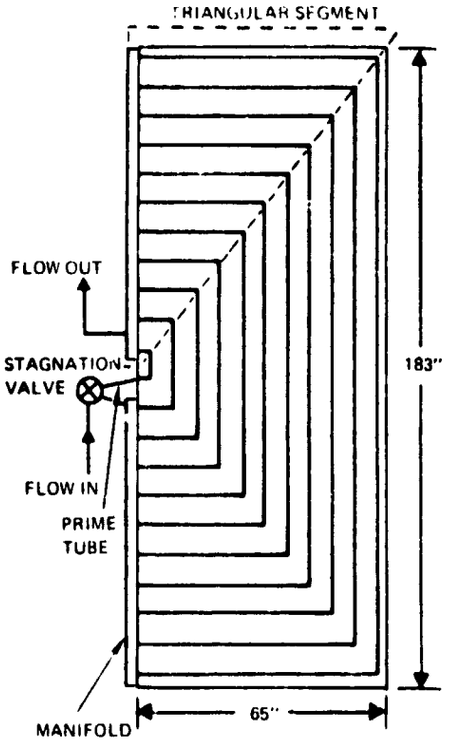

FIGURE 1 WIDE HEAT LOAD RANGE RADIATOR TUBE LAYOUT

the flow regime which would prevail along the condensation path. The method developed by Baker (Reference [10]) was used to do this as explained in Appendix A.

Two condensing radiator panels were fabricated as shown in Figure 2, and as described in Appendix A and in Reference [11]. A dry expansion evaporator was designed and built as shown in Figure 3. The hybrid refrigeration system was assembled with the two radiator/condenser panels installed in the VSD Space Environment Simulator. A schematic of the system is shown in Figure 4, and photographs of the installation are given in Figures 5 - 8. Testing of the system was accomplished under both atmospheric and vacuum conditions as described in Reference [8]. Typical operating conditions are given in Tables 1 and 2.

Results of the testing were entirely satisfactory. Typical temperature profiles along the length of the tube are shown in Figures 9-12. Figures 9 and 10 clearly show the break-point in the temperature profile which occurs at the point of complete condensation. While a two-phase condition is maintained the fluid temperature is a function of the saturation pressure, and falls slightly in the direction of flow due to flow pressure drop. When a single-phase flow is established, then the temperature is independent of pressure, and so falls in proportion to the panel heat transfer rate. The predicted temperatures compare favorably with the data; the abrupt temperature changes in the predictions near the entrance are a result of longitudinal conduction not being considered in the mathematical model. The large temperature drop results from the small heat transfer coefficient near the end of the superheated gas flow section of the condenser. As condensation starts in the two-phase flow region, heat transfer to the tube increases dramatically.

Pressure drop predictions were generally higher than the data with an error of generally less than 20% as shown in Table 3. This is good correlation for two-phase flow pressure drop (Reference [8]).

There were no signs of flow instability in these tests. Runs were made with the radiator panels tilted and with vibration imposed on the panel in attempts to induce flow instability. At no time was there any indication of such instabilities, however, the nature of the test hardware and instrumentation could obscure instabilities.

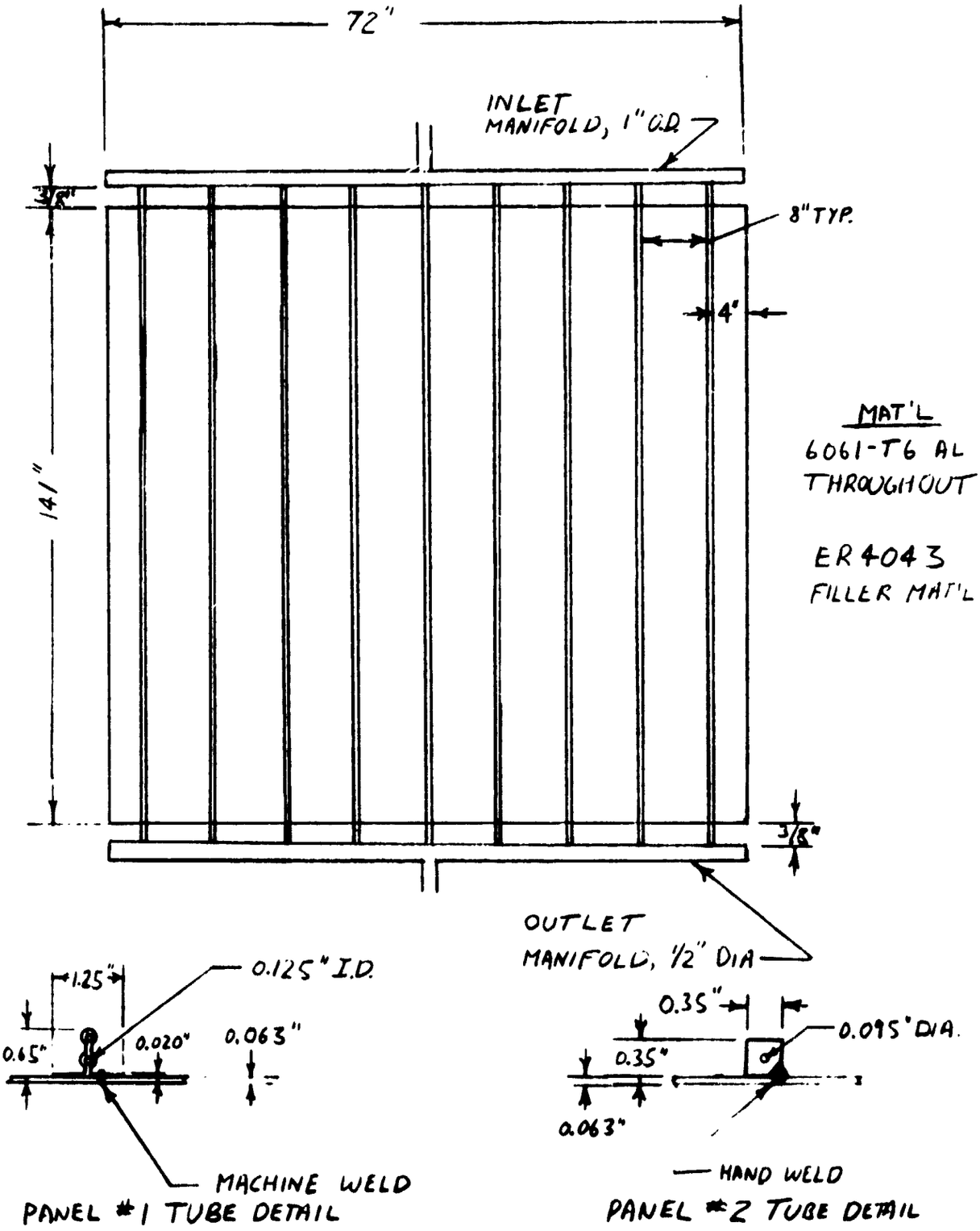

FIGURE 2 CONDENSER/RADIATOR DESIGN

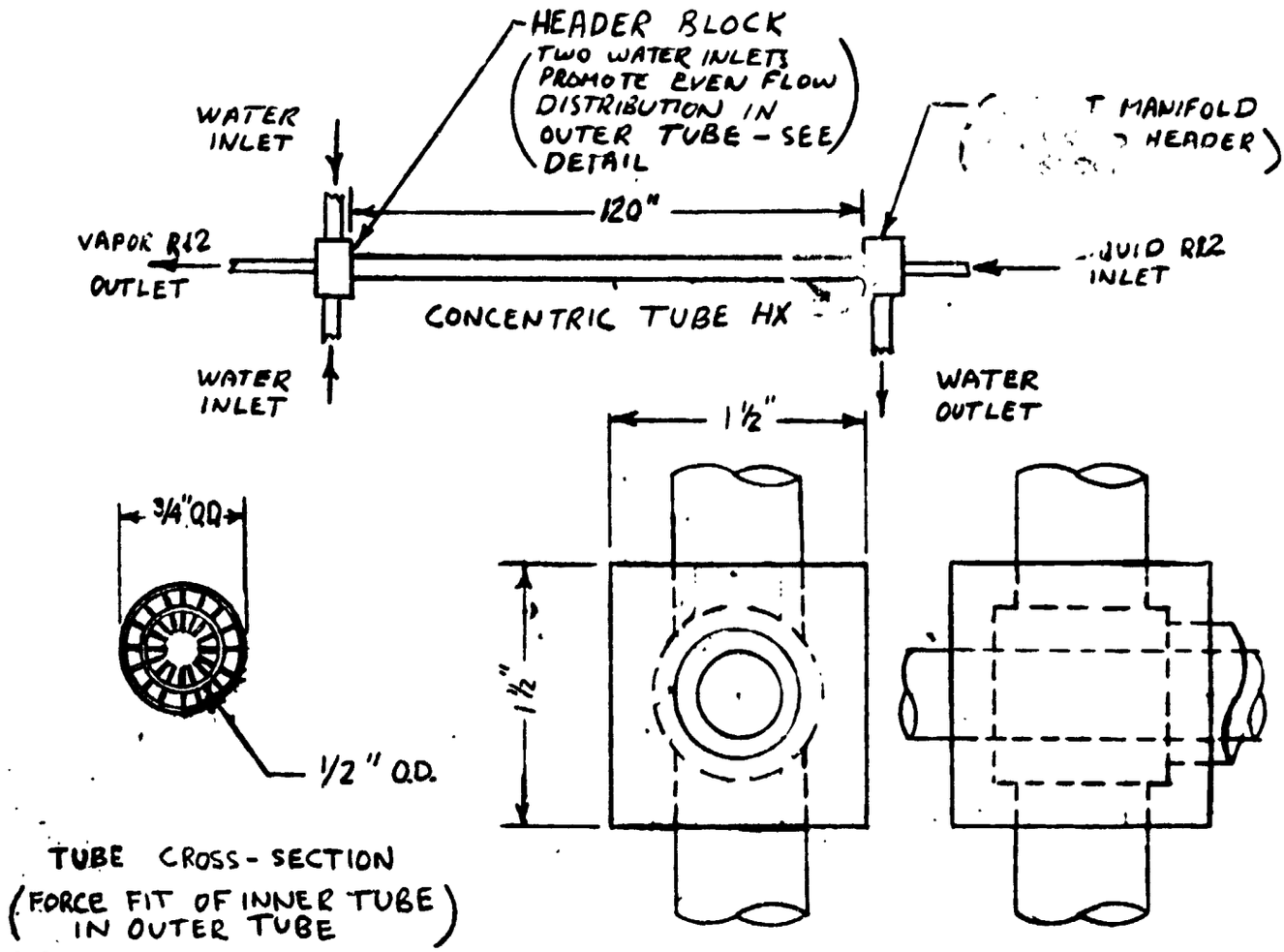

HEADER BLOCK CONFIGURATION

TUBE DIMENSIONS		
PARAMETER	OUTER	INNER
O.D.	0.75"	0.50"
WALL THICKNESS	0.033"	0.041"
NO. OF FINS	16	16
FIN THICKNESS	0.020"	0.020"
FIN DEPTH	0.088"	0.067"
FIN CONFIGURATION	SPIRAL	SPIRAL

FIGURE 3 EVAPORATOR/INTERCOOLER DESIGN

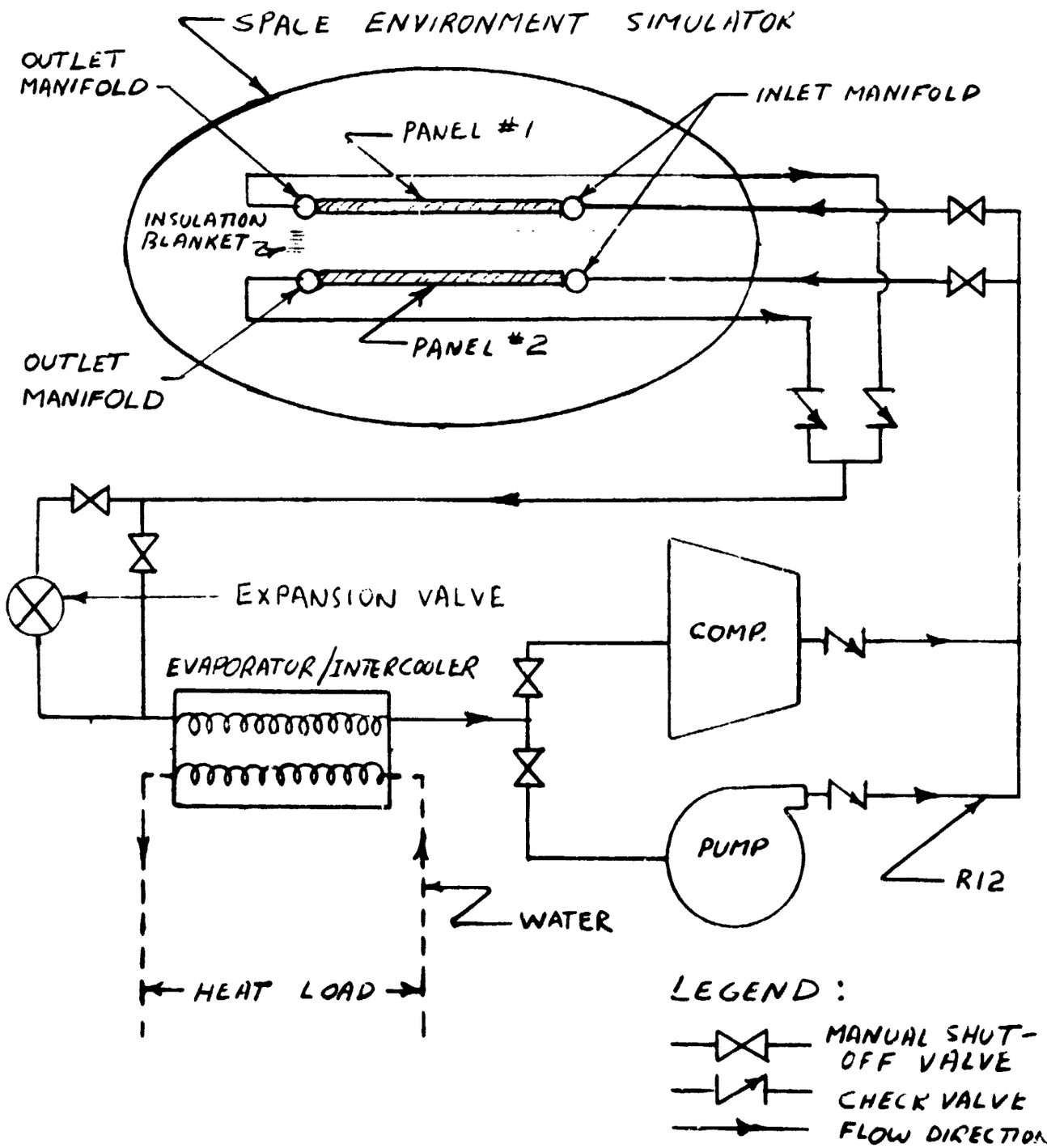

FIGURE 4 TEST SET-UP

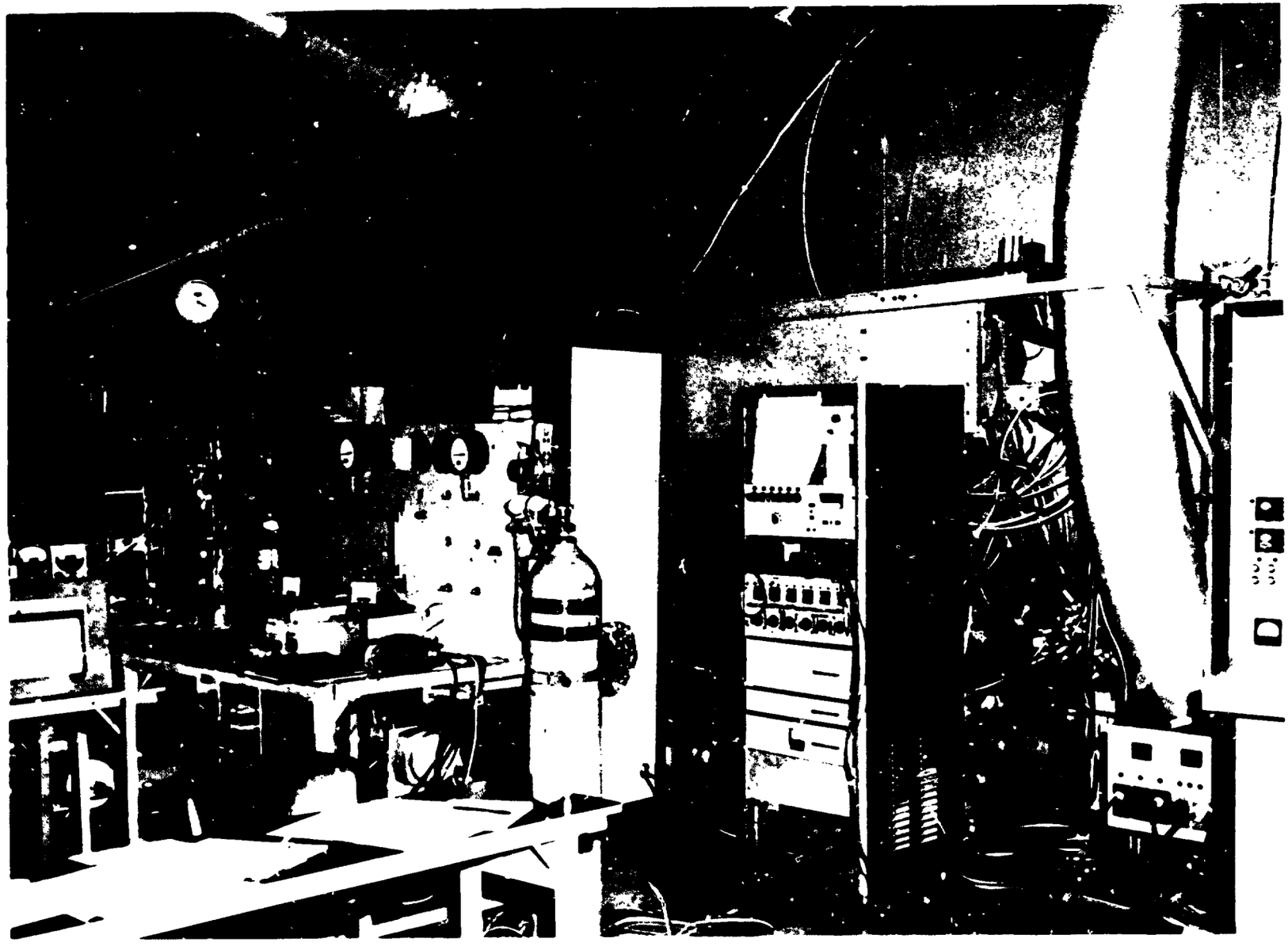

FIGURE 5 View of the Test Set-up Showing the system instrumentation with the Space Environment Simulator as a background

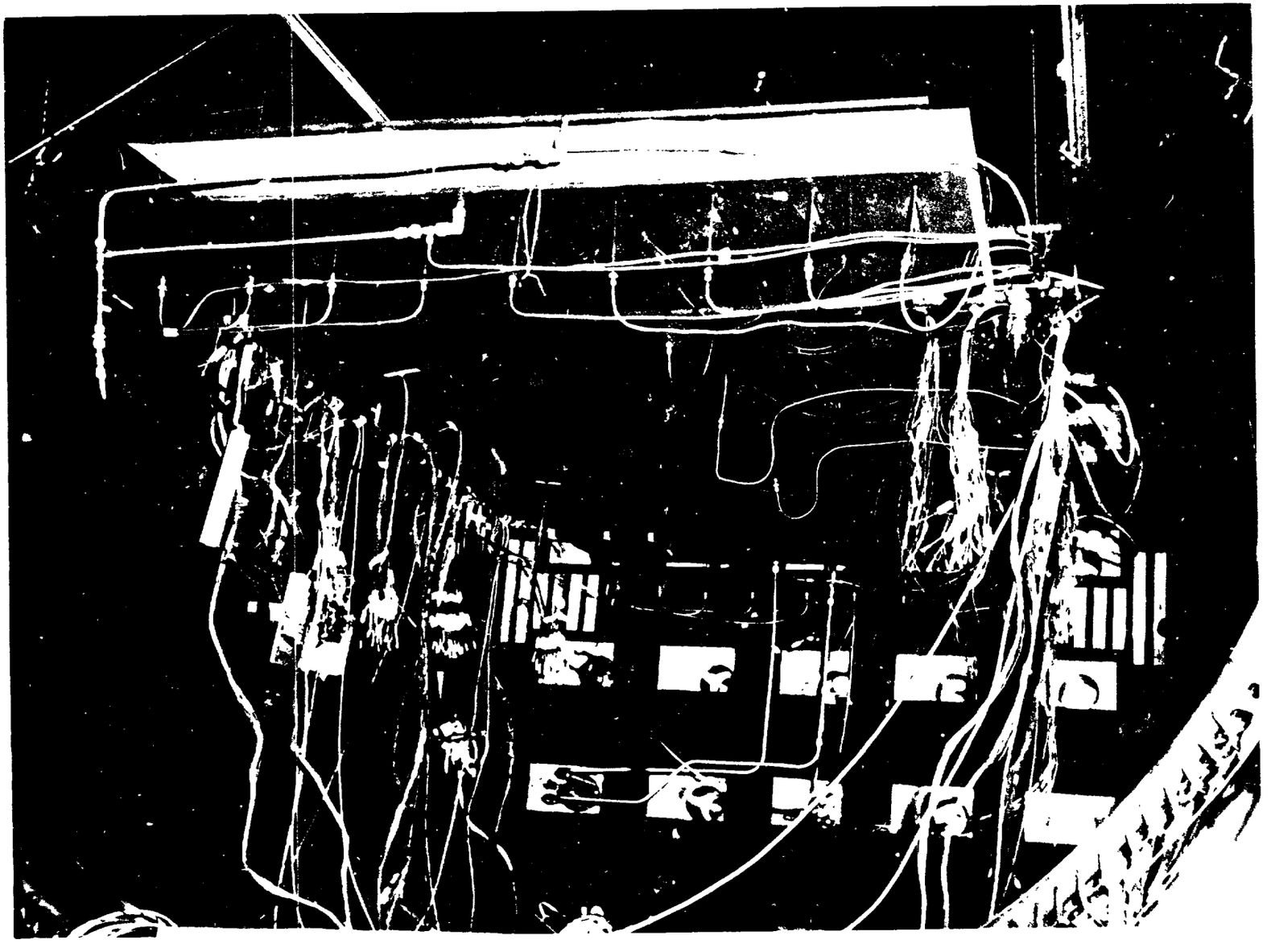

FIGURE 1 The Two Candidate Radiator/Condenser Panels are shown mounted in the Crew Environment Simulator for atmospheric testing

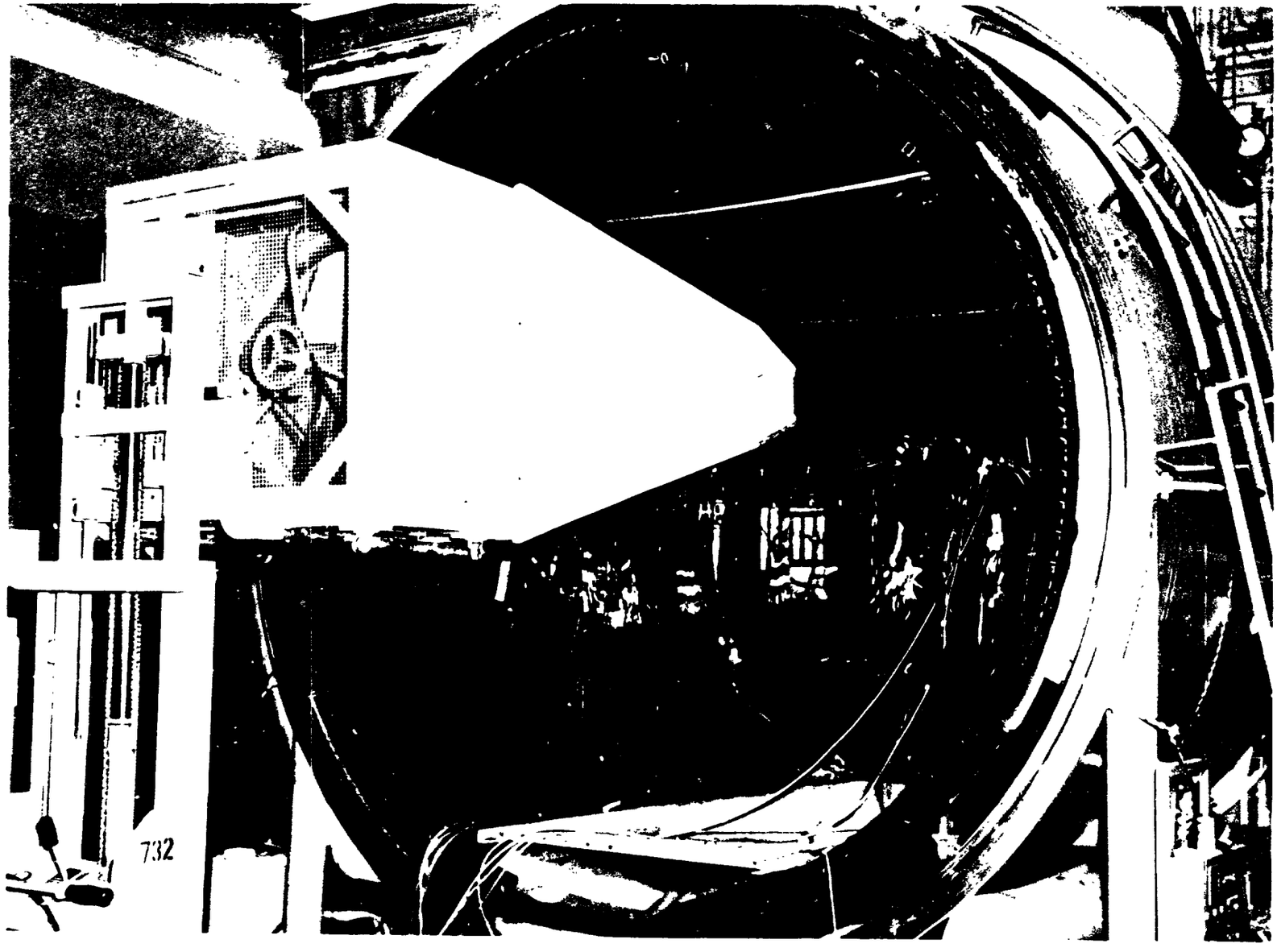

FIGURE 7 The Fan and Diffuser used to provide cooling to the Radiator/ Condenser Panels During Atmospheric Testing are shown in Position

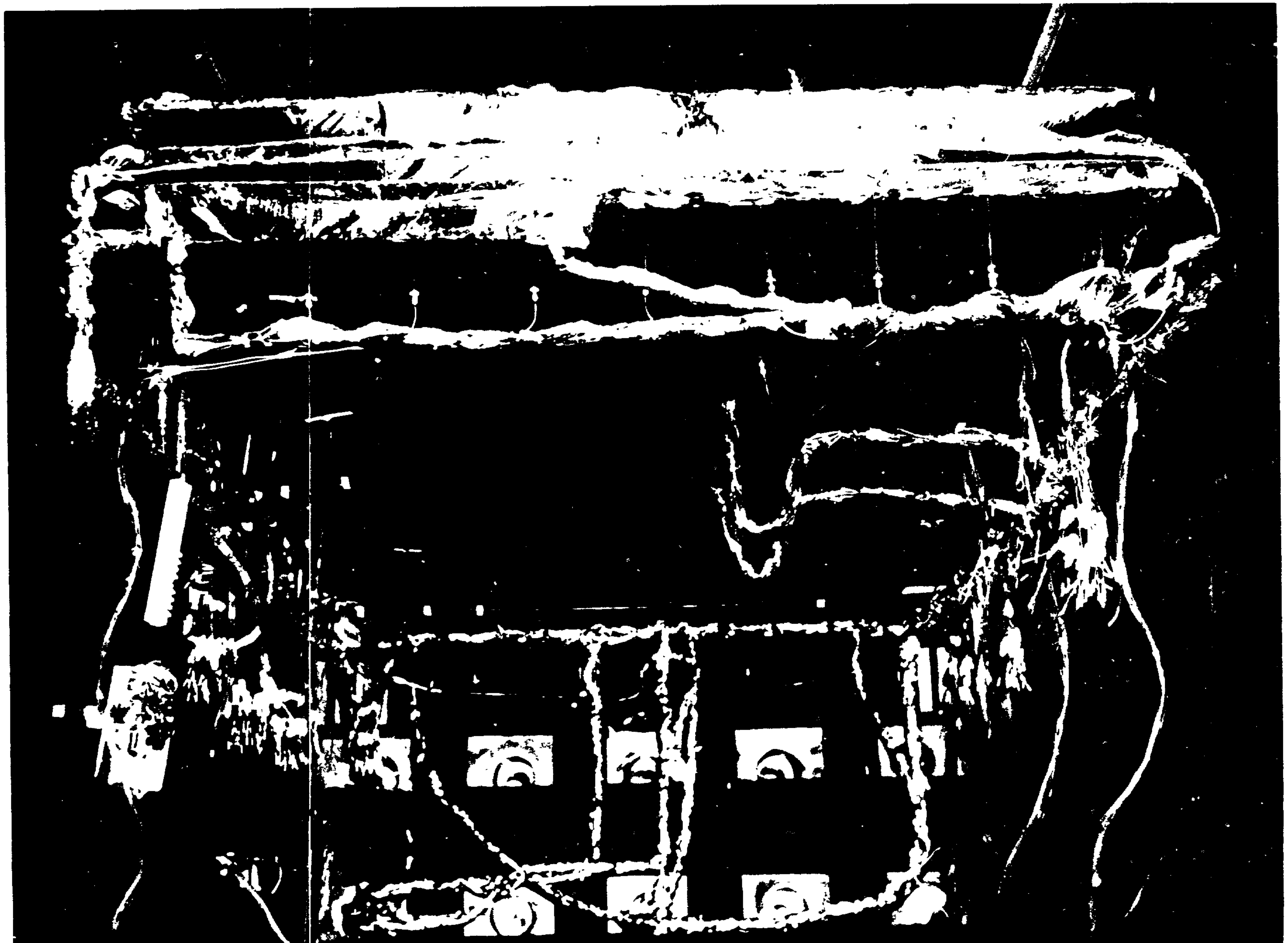

[illegible] 1. The [illegible] Sensor Levels are shown with Insulation used in [illegible] Testing in Place

TABLE 1

NOMINAL OPERATING CONDITIONS FOR REFRIGERATION SYSTEM MODE TESTS

Refrigerator	
Refrigerant	R12
COP	1.75
Condenser Temperature	140°F (p = 221.32 psia)
Evaporator Temperature	40°F (p = 51.67 psia)
Evaporator Heat Load	6500 BTU/HR
Condenser Heat Rejection	11300 BTU/HR
Compressor Gas Outlet Temperature	160°F
Refrigerant Flowrate	180 LB/HR
Condenser Sink Temperature	-300°F
Evaporator/Intercooler Heat Load Flow Loop	
Heat Transport Fluid	Water
Inlet Temperature	100°F
Outlet Temperature	87°F
Flowrate	500 LB/HR

TABLE 2

NOMINAL OPERATING CONDITIONS FOR PUMPED FLUID RADIATOR MODE TESTS

Radiator

Transport Fluid	R12
Inlet Temperature	140°F
Outlet Temperature	40°F
Flowrate	400 LB/HR*
Heat Rejection	8000 BTU/HR
Sink Temperature	-300°F
Pump Outlet Pressure	150 psia

Evaporator/Intercooler Heat Load Flow Loop

Transport Fluid	Water
Inlet Temperature	180°F
Outlet Temperature	164°F
Flowrate	500 LB/HR

* This yields R12 flow at 44.5 LB/HR/TUBE for 9 parallel tubes on a 0.063 inch sheet with 8 inch centers across a 6 ft span which is essentially equivalent to the intended two-dimensional Modular Radiator System Test Condition for R21 flow through twelve tubes on a 0.020 inch sheet with 6 inch centers, Reference 5.

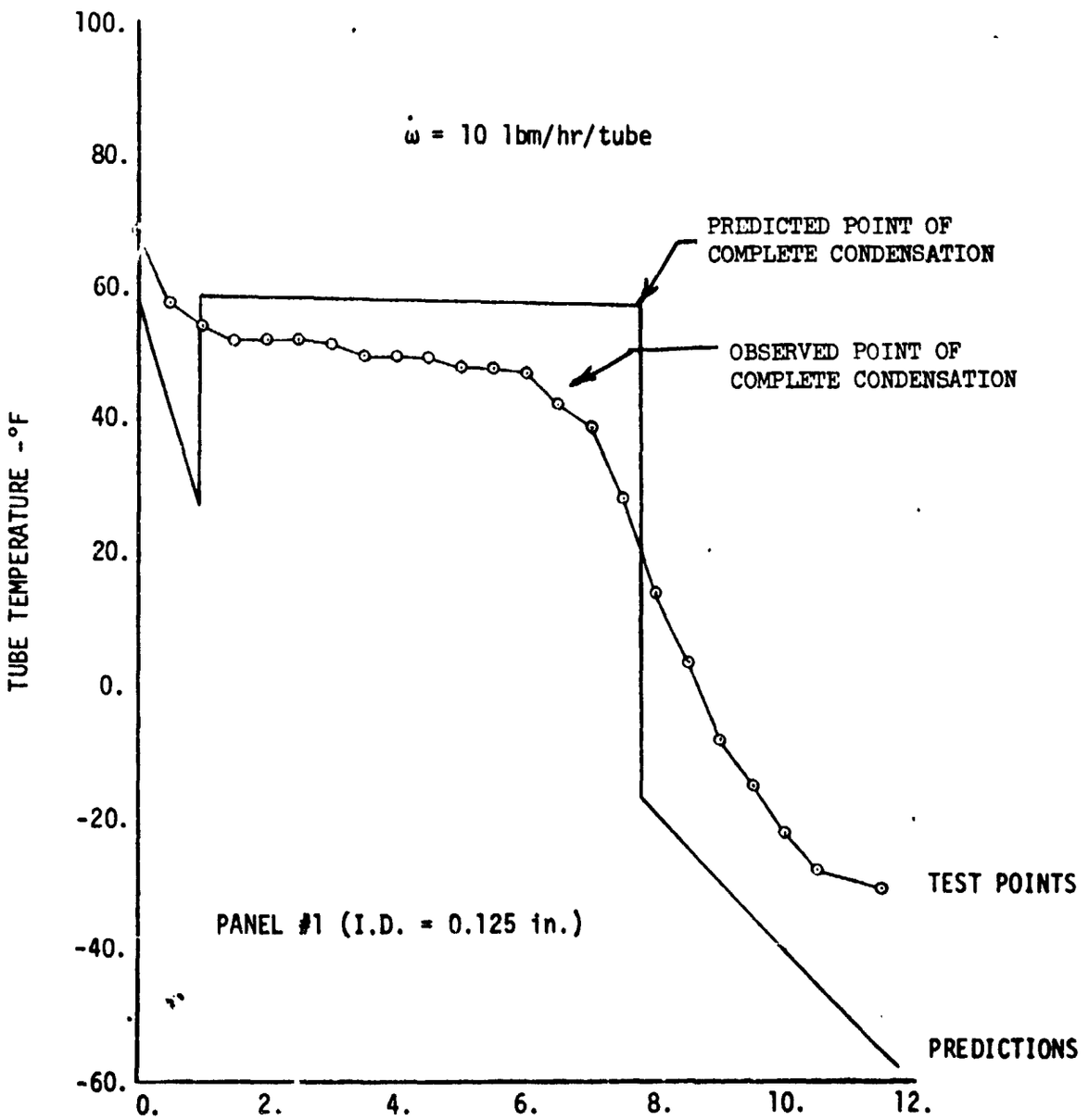

FIGURE 9 RC PANEL TEMPERATURE PROFILE - LOW LOAD
(EVAPORATOR LOAD = 3650 BTU/HR)

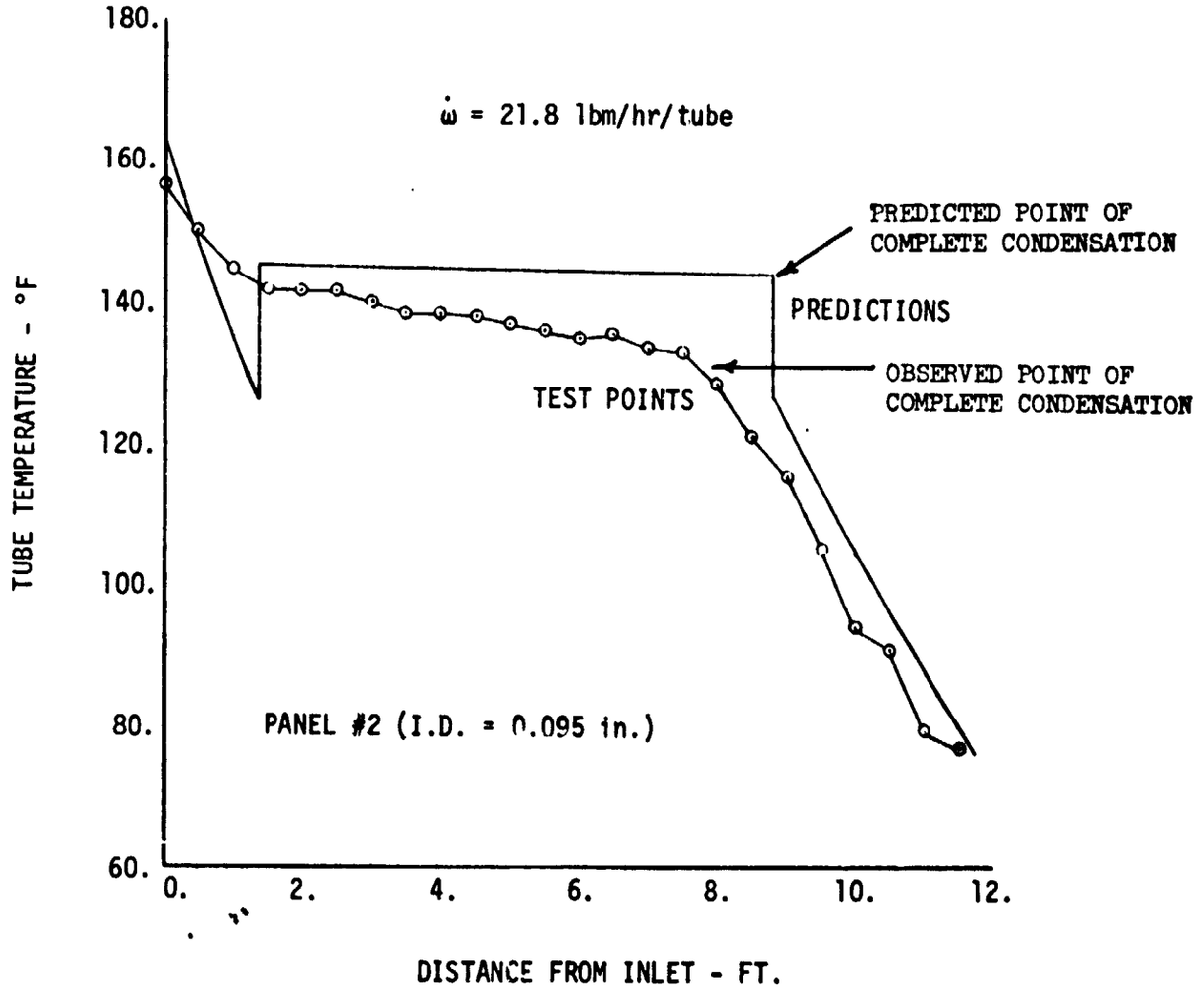

FIGURE 10 RC PANEL TEMPERATURE PROFILE
(EVAPORATOR HEAT LOAD = 9250 BTU/HR)

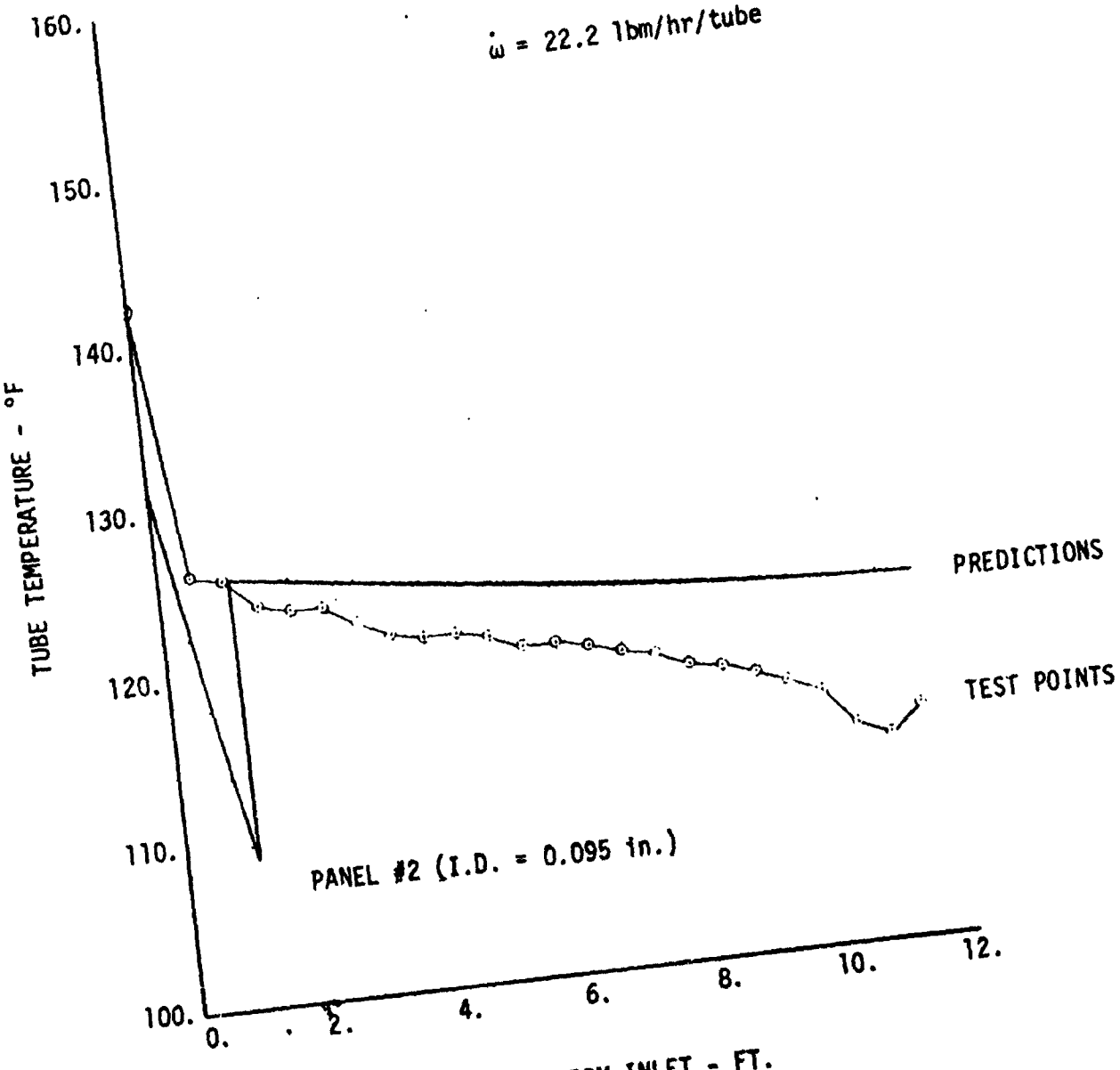

FIGURE 11 RC PANEL TEMPERATURE PROFILE
(EVAPORATOR HEAT LOAD = 10,100 BTU/HR)

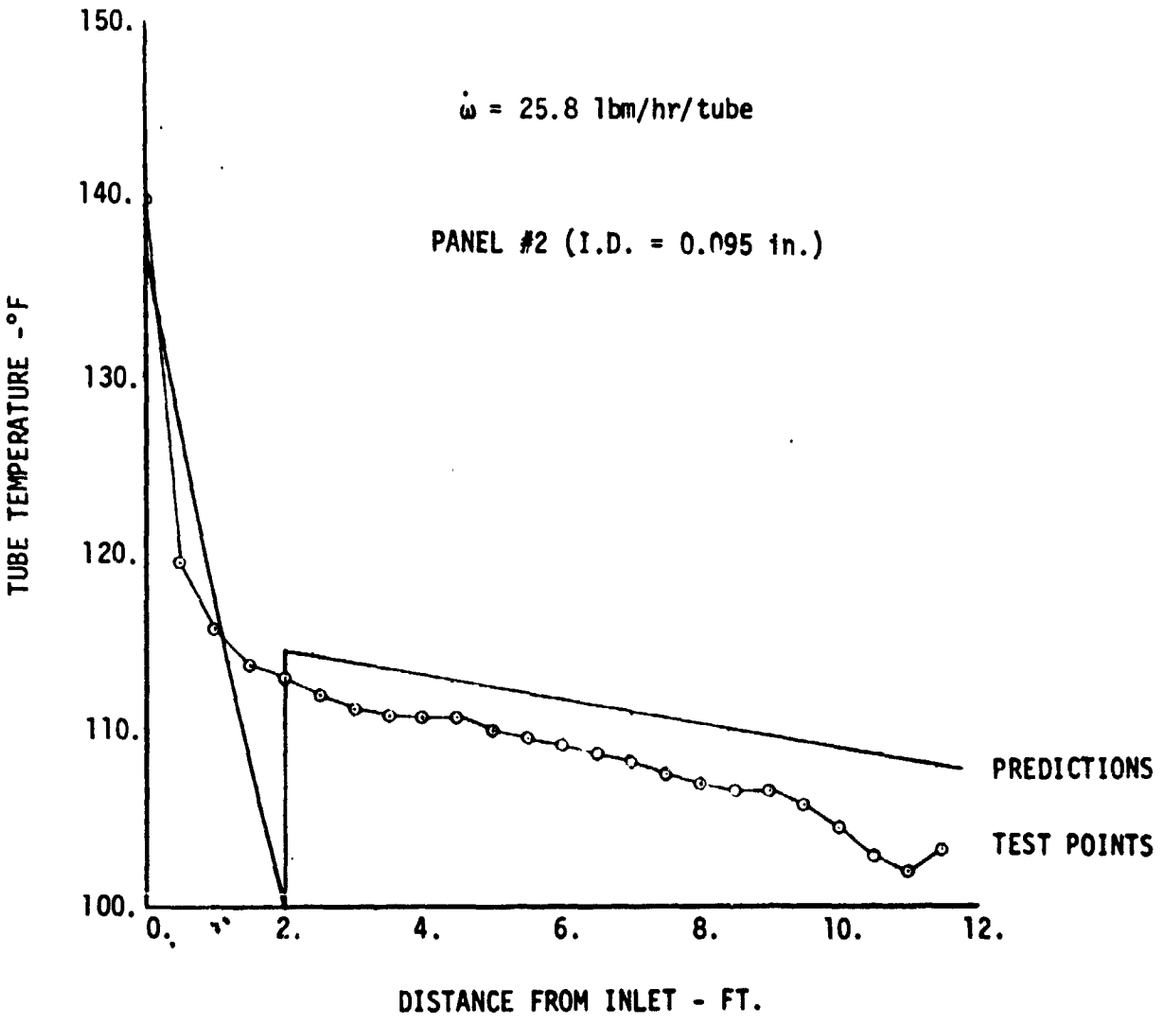

FIGURE 12 RC PANEL TEMPERATURE PROFILE
(EVAPORATOR LOAD = 9180 BTU/HR)

TABLE 3

PRESSURE DROP CORRELATION

PANEL NO.		P_{IN}	T_{IN}	$\dot{\omega}_{F-12}$	ΔP_{CAL}	ΔP_{TEST}	ERROR
#1	#2	PSIG	°F	lbm/hr	PSI	PSI	%
X		167	126	21.4	2.9	2.8	3.6
X		152	118	20.0	2.9	2.5	16.0
X		172	178	18.2	2.1	1.7	23.4
X		123	152	16.9	2.1	1.7	23.4
X		205	181	23.1	2.8	2.4	16.7
	X	237	185	25.4	11.5	8.4	37.0
	X	240	150	26.7	10.4	8.9	16.8
	X	168	157	20.0	10.1	7.0	43.1
	X	193	152	20.0	8.5	8.4	1.2
	X	134	132	16.7	7.4	7.2	2.8

PANEL #1 - TUBE I.D. = 0.125 in.

PANEL #2 - TUBE I.D. = 0.095 in.

ΔP_{CAL} - CALCULATED PRESSURE DROP

ΔP_{TEST} - ACTUAL PRESSURE DROP

P_{IN} - RC PANEL INLET PRESSURE

T_{IN} - RC PANEL INLET TEMPERATURE

W_{F-12} - REFRIGERANT FLOWRATE

The overall performance of the system was within expected bounds. Figure 13 shows the Coefficient of Performance (COP) measured in the system as a function of compression ratio compared to prediction. There is excellent agreement here; at the low shaft speeds (200 rpm) the efficiency of the compressor falls considerably below optimum, as the data shows. The prediction is for optimum compressor speed at each load condition. It should be noted that this curve gives COP exclusive of the drive motor. Figure 14 shows a performance map for the system tested.

The last objective of the test was to demonstrate that switchover from the single-phase ("radiator") mode of operation to the two-phase ("refrigeration") mode and vice versa could be made routinely without damage to the system. Numerous switchovers were made according to the operational procedures developed in the test plan, and no difficulty was encountered, nor was any damage to hardware sustained.

Finally, a considerable amount of experience in operating the hybrid refrigeration system was obtained.

The systems test is discussed in much greater detail in Reference [11].

2.2 Zero-G Experiment

The system tests left unanswered the questions regarding heat transfer rate, pressure drop, and flow stability of condensing flow of a wetting fluid in a zero-gravity field. In order to increase confidence in the design, and to reduce technical risk, it was decided to design an experiment to verify the analyses in simulated zero-gravity.

An investigation of the various means of achieving simulated zero-gravity was conducted, and it was decided that the most suitable approach was through the use of an aircraft flying parabolic trajectories. This approach can produce low acceleration conditions for periods of up to 30 seconds.

The experimental approach which evolved was to film the condensing fluid flow with a high speed camera in local regions, and to examine the flow down the entire length of a tube visually.

The design of the zero-g test apparatus is discussed in detail in Reference [12]. The system was designed for an operating pressure of 1.72 MPa (250 psia) at a temperature of 378°K (220°F), with delivery flowrates up to 25 g/s (200 lb/hr). The system was tested operating in steady state at

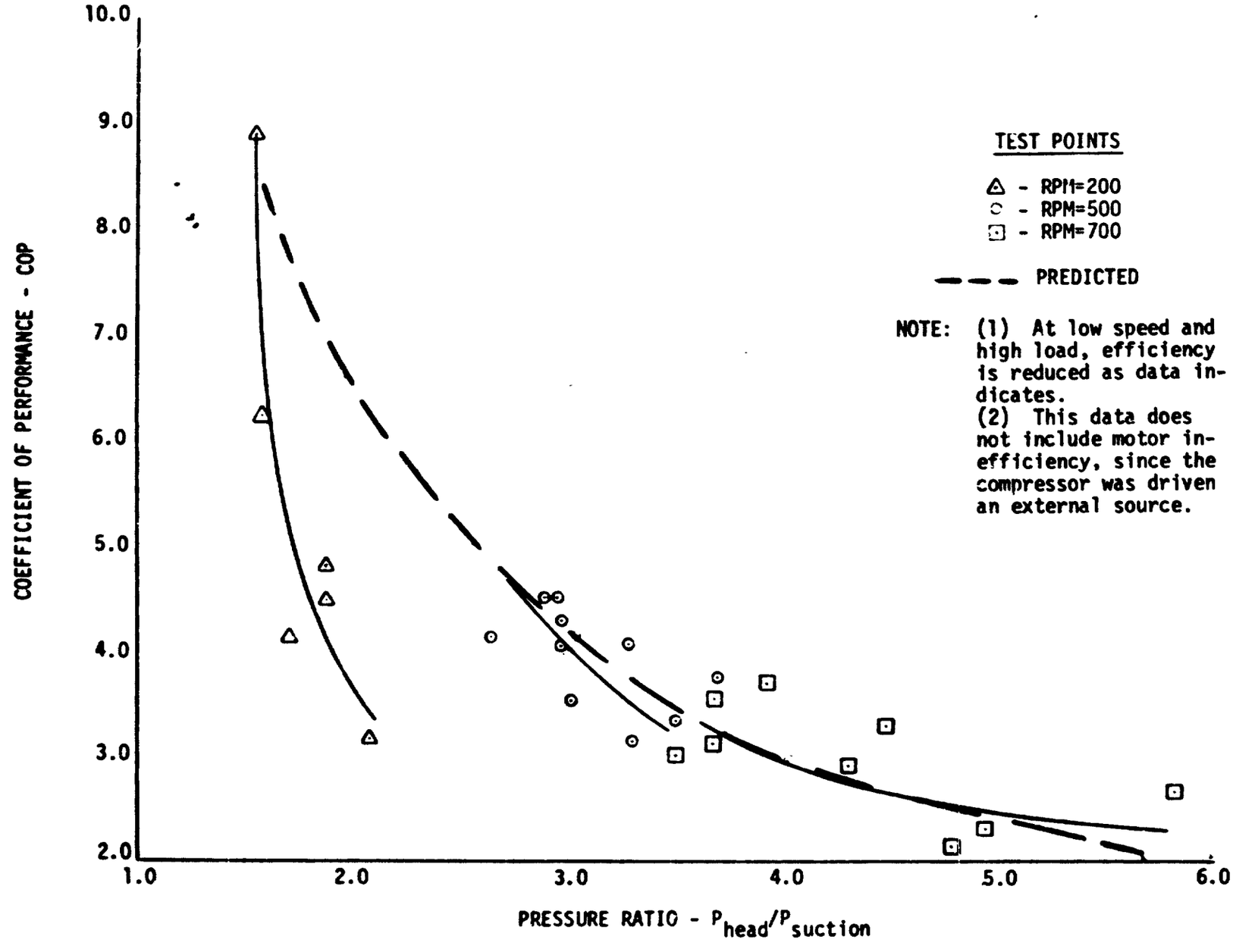

FIGURE 13 COEFFICIENT OF PERFORMANCE VS PRESSURE RATIO

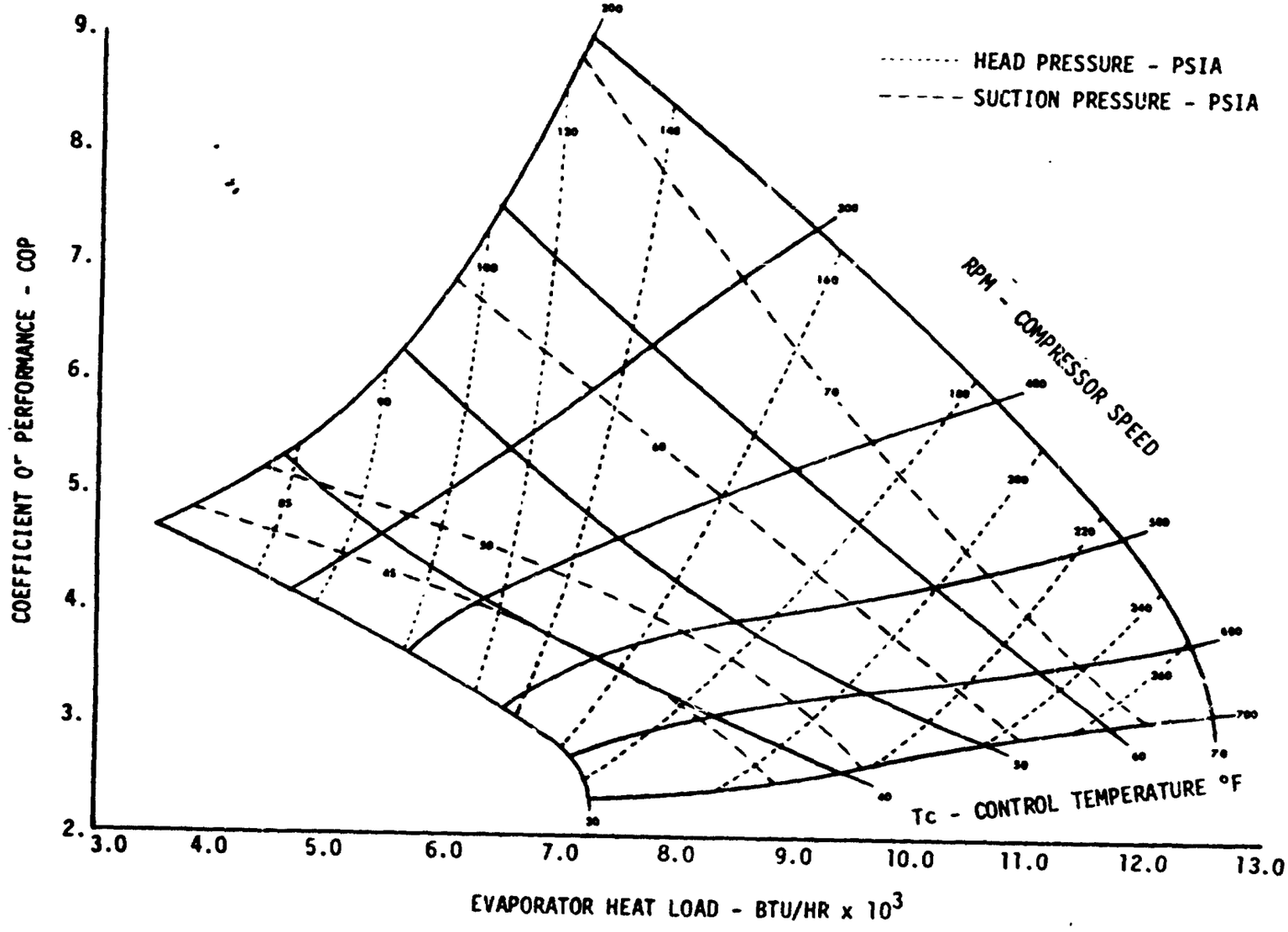

FIGURE 14 PERFORMANCE MAP WITH OPERATING PRESSURES

pressures up to 1.64 MPa (238 psia), and was operated in a transient up to a pressure of 2.07 MPa (300 psia) where pressure relief valve operation was verified.

Three fused quartz tubes from the lot used in the flow visualization apparatus were pressurized to failure; all burst at a pressure of greater than 13.8 MPa (2000 psia). The freon tank was fabricated to ASME unfired pressure vessel code, and was proofed to 4.13 MPa (600 psi). The gas receiver was designed for a burst pressure of 6.89 MPa (1000 psi) and was proof-tested at 3.45 MPa (500 psi). The structure of the test apparatus was designed for loads of 16 g's forward along the longitudinal axis, 5 g's down and 2 g's in other directions. Figures 15-20 show the test apparatus in some detail.

The tests conducted on the zero-g condensation experiment apparatus are described in detail in Reference [13], and are also described in Appendix A. The flight tests are described in detail in Reference [14] and in Appendix A. Results of these tests are discussed in Appendices A and B.

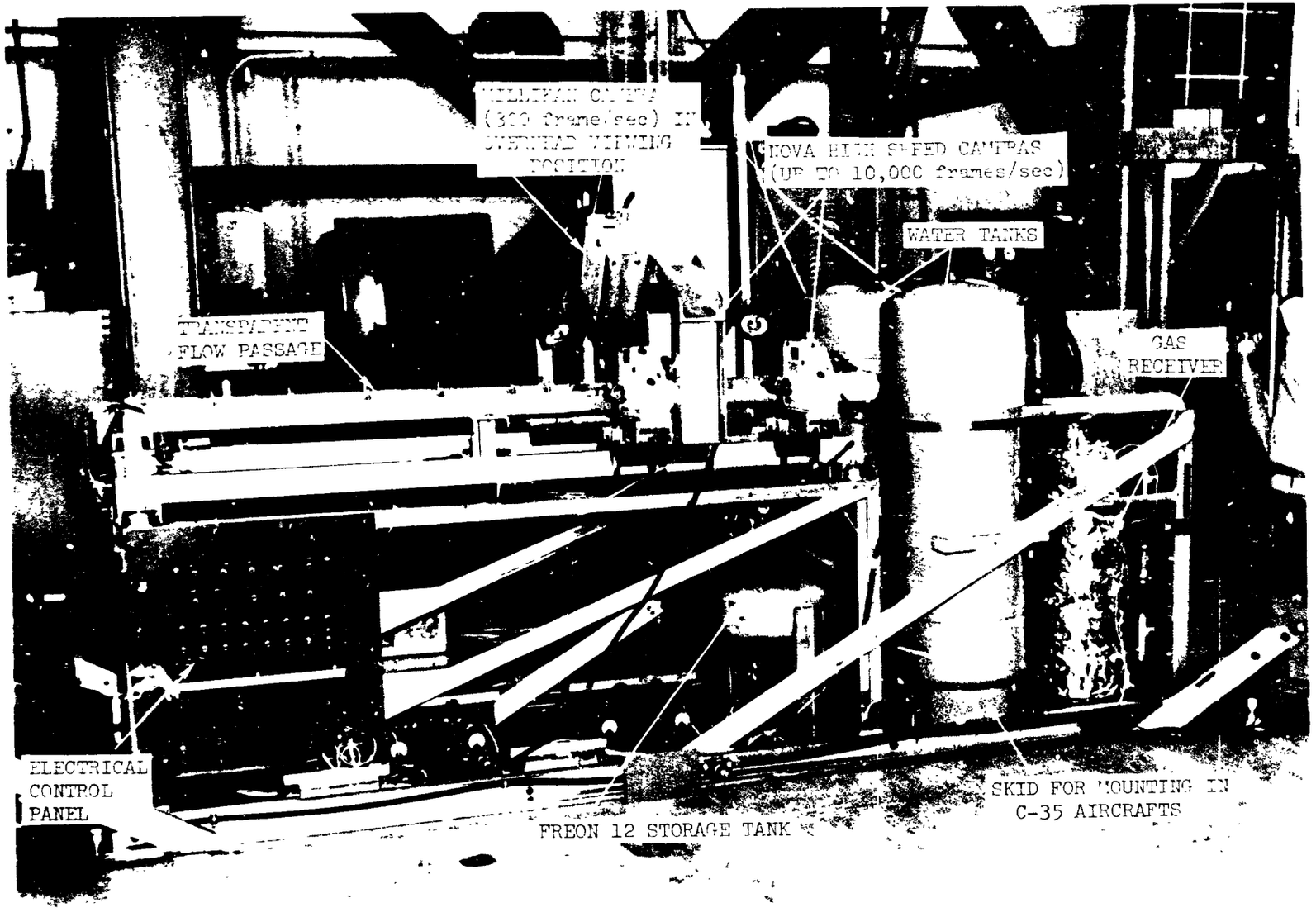

FIGURE 15 SIDE VIEW OF ZERO-G EXPERIMENT APPARATUS

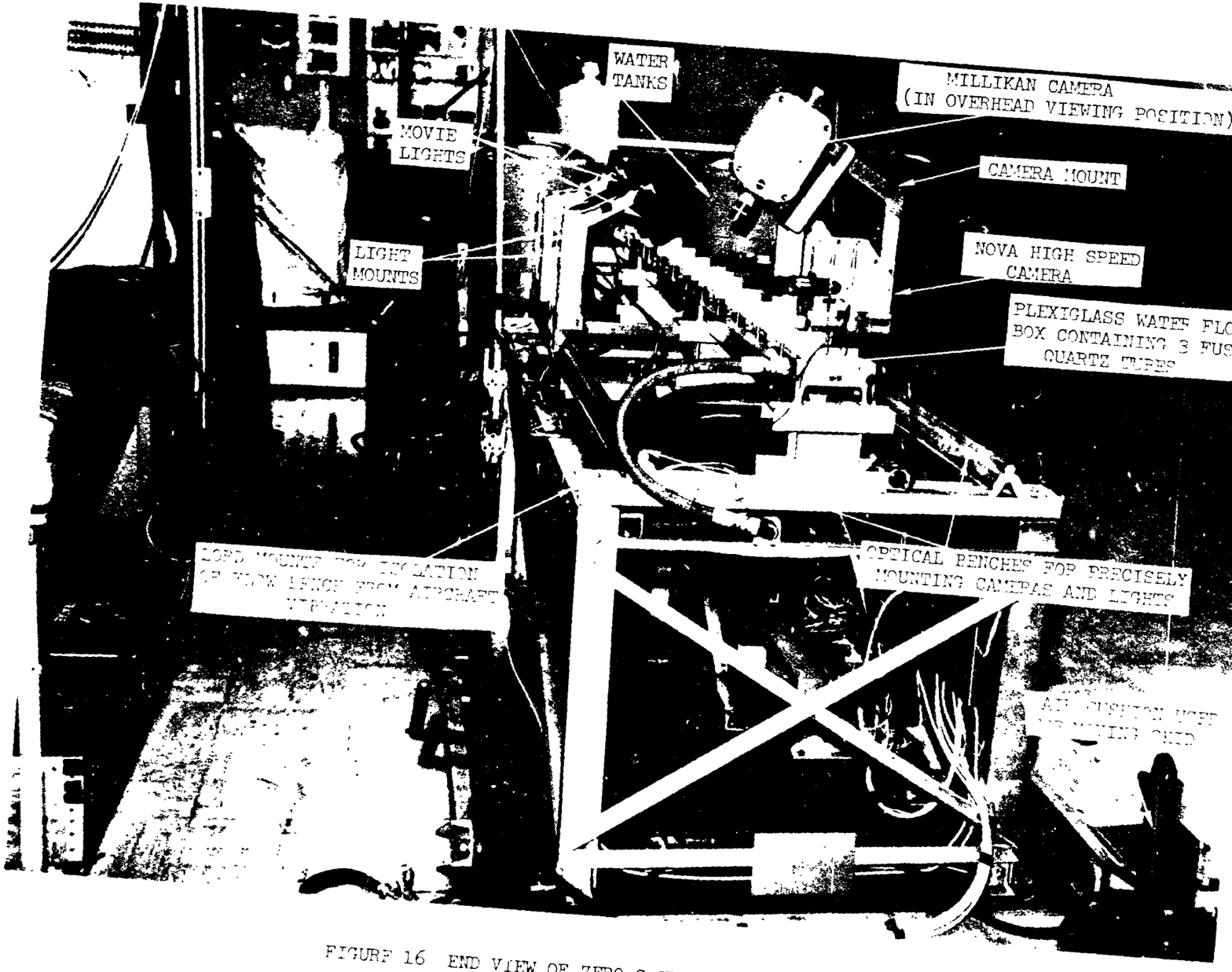

FIGURE 16 END VIEW OF ZERO-G EXPERIMENT APPARATUS

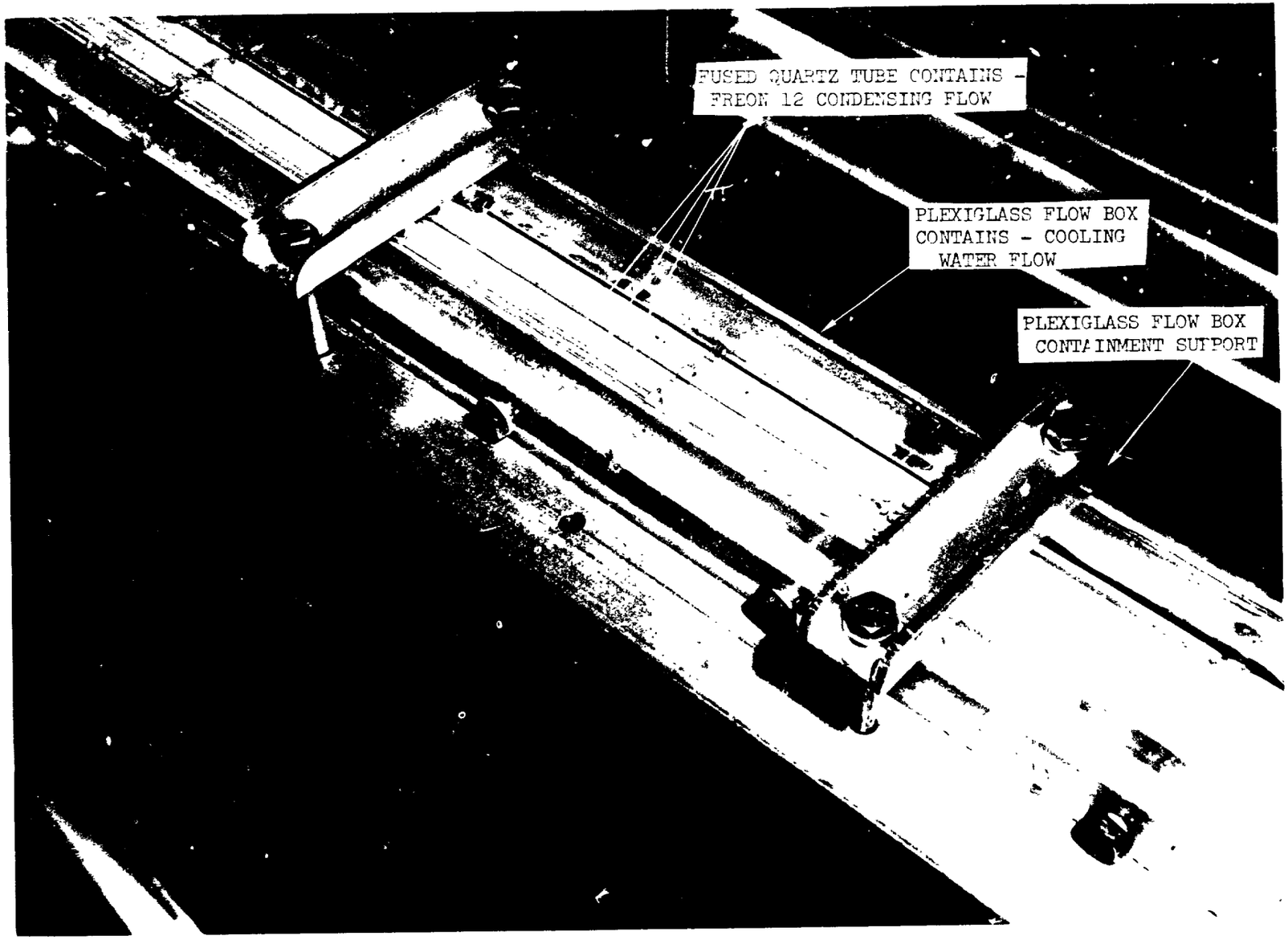

FIGURE 17 CLOSE-UP VIEW OF PLEXIGLASS FLOW BOX

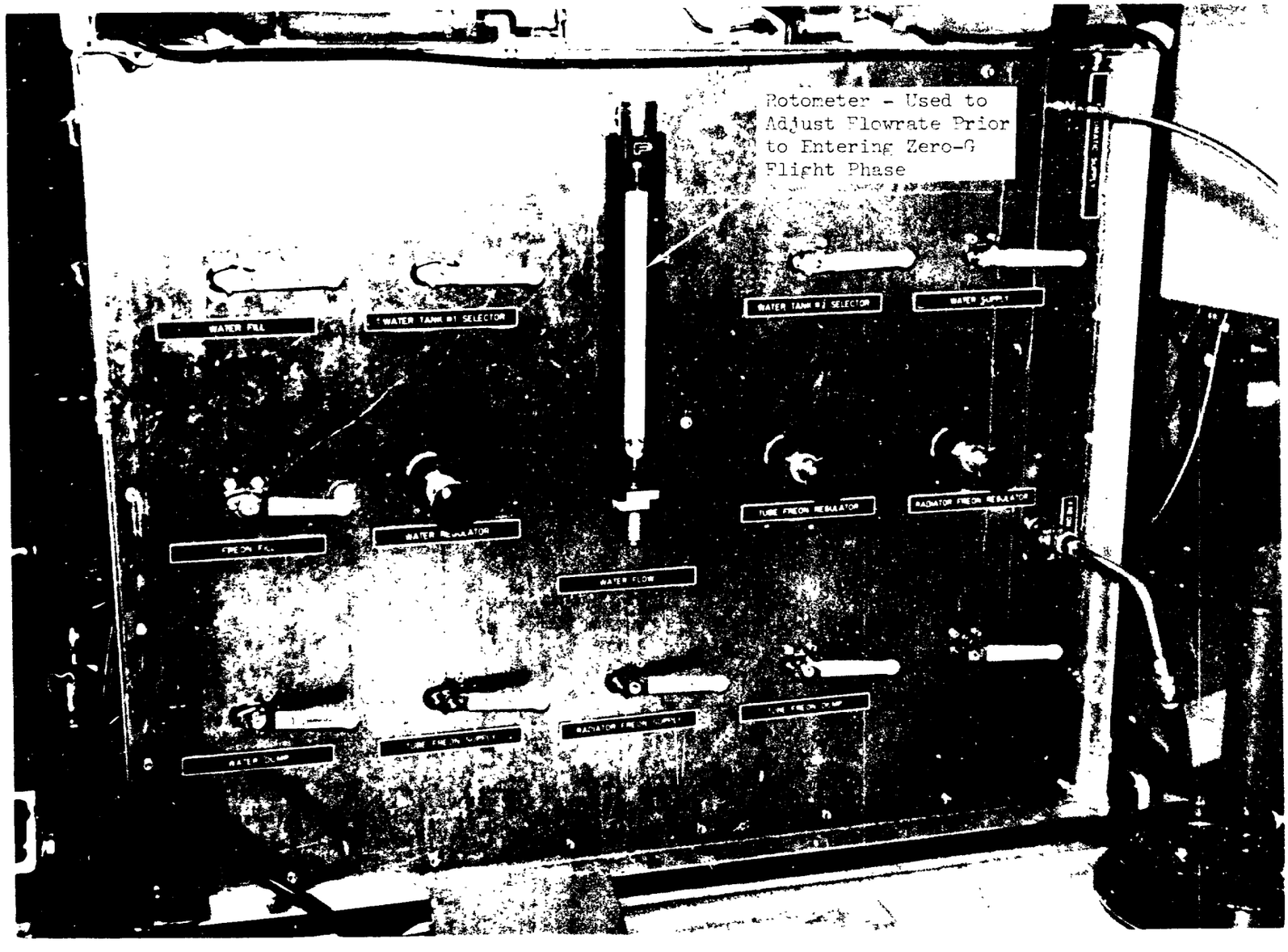
Rotometer - Used to
Adjust Flowrate Prior
to Entering Zero-G
Flight Phase
WATER FILL
WATER TANK #1 SELECTOR
WATER TANK #2 SELECTOR
WATER SUPPLY
WATER REGULATOR
TUBE FREON REGULATOR
RADIATOR FREON REGULATOR
WATER FLOW

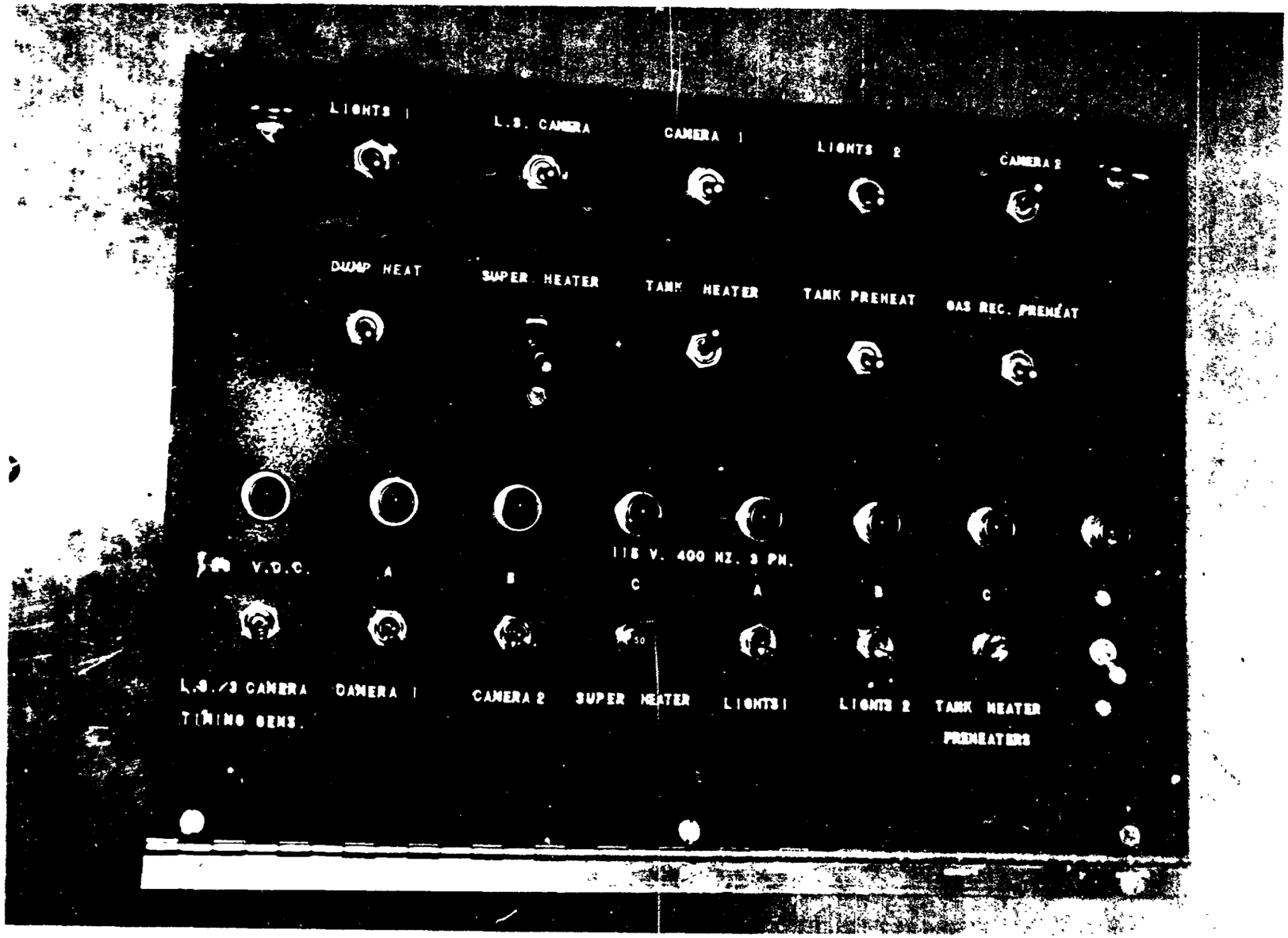
LIGHTS 1
L.S. CAMERA
CAMERA 1
LIGHTS 2
CAMERA 2
DUMP HEAT
SUPER HEATER
TANK HEATER
TANK PREHEAT
GAS REC. PREHEAT
V.D.C.
A
B
C
115 V. 400 HZ. 3 PH.
A
B
C
L.S./3 CAMERA TIMING GENS.
CAMERA 1
CAMERA 2
SUPER HEATER
LIGHTS 1
LIGHTS 2
TANK HEATER PREHEATERS

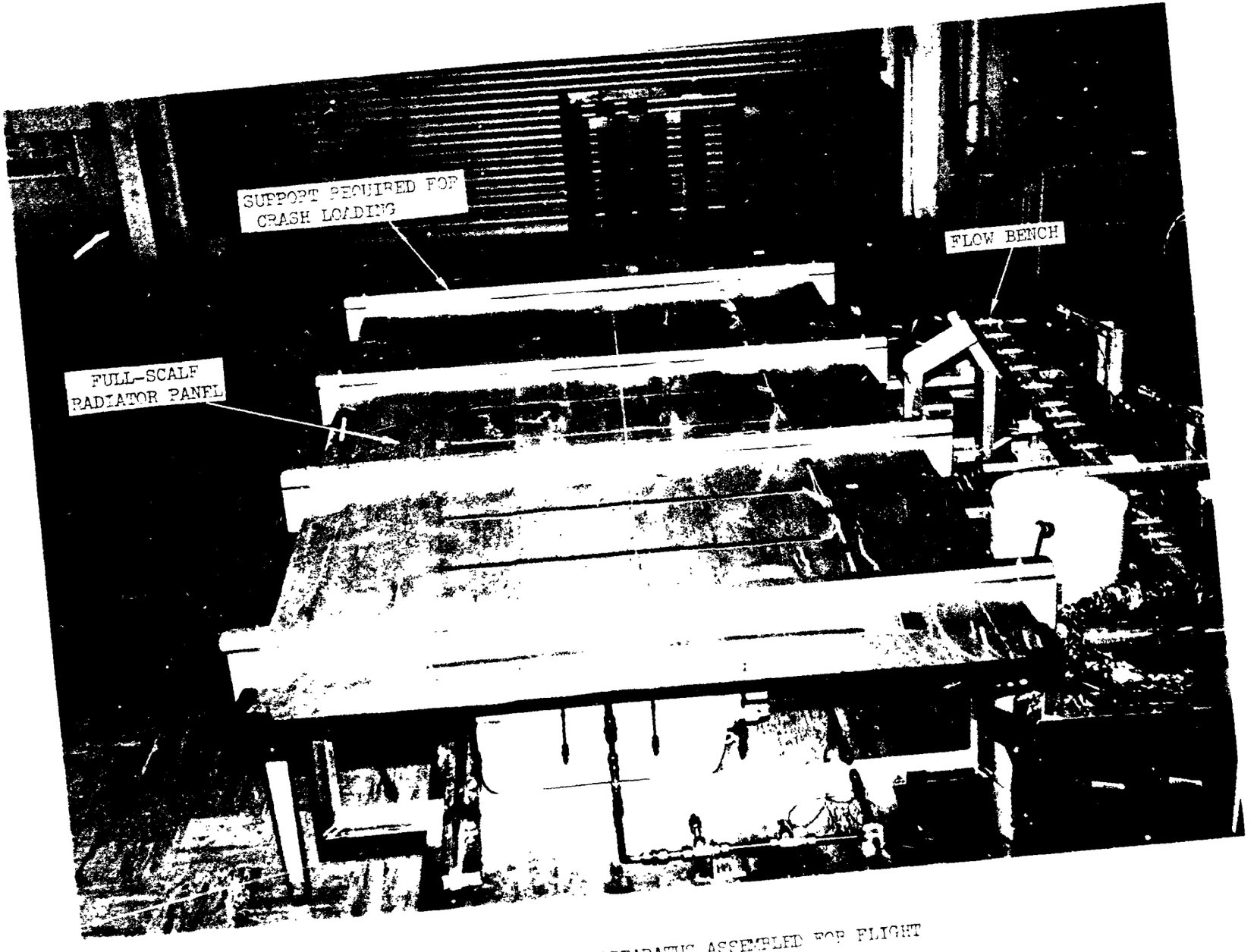

FIGURE 20 ZERO-G APPARATUS ASSEMBLED FOR FLIGHT

3.0 CONCLUSIONS AND RECOMMENDATIONS

3.1 Conclusions

The primary conclusions of this work are:

(1) The hybrid conventional radiator/vapor cycle heat rejection system is feasible.

(2) Operation of a spacecraft refrigeration system is feasible.

(3) Flow regime (e.g., annular, slug, bubble, etc.) in condensing flow in zero-g can be predicted reasonably well with the Baker plot.

(4) Condensing flow heat transfer rates and friction pressure drops do not appear to be degraded under zero-g conditions, and are reasonably well predicted using conventional techniques.

(5) Condensing radiator can be designed so that hydrodynamically stable flow conditions prevail.

3.2 Recommendations

The following recommendations are made relative to this work:

(1) Additional simulated zero-g experiments should be conducted under more carefully controlled conditions and with better instrumentation.

(2) Data taken in simulated zero-g conditions should be used to improve techniques for calculating heat transfer rates and pressure drop. The photographic data taken in the subject tests clearly shows that the flow models used in conventional correlations are not correct.

(3) Attention should be directed to the practical design of other system components for use in zero-gravity, including the dry-expansion evaporator and compressor lubrication.

4.0 REFERENCES

[1] Copeland, R. J., T. D. Blount, and J. L. Williams, "Evaluation and Selection of Refrigeration Systems for Lunar Surface and Spacecraft Applications", VSD Report T122-RP-004, dated 31 October 1971.

[2] Blount, T. D. and J.L. Williams, "Development of A Refrigeration System for Lunar Surface and Spacecraft Applications - Progress Report" VSD Report No. T122-RP-006, dated 3 September 1971.

[3] Wiggins, C. L., H. R. Howell, and J. L. Williams, "Development of a Refrigeration System for Lunar Surface and Spacecraft Applications"- Progress Report, VSD Report No. T122-RP-008, dated 1 November 1971.

[4] Tufte, R. J., "Wide Heat Load Range Space Radiator Development", ASME paper 71-Av-5, dated 14 July 1971.

[5] Dietz, J. B., M. L. Fleming, and R. J. Tufte, "Modular Radiator System Development for Shuttle and Advanced Spacecraft", ASME Paper 72-ENAv-34, dated 16 August 1972.

[6] Fleming, M. L., H. R. Howell, J. B. Dietz, and M. W. Reed, "Shuttle Active Thermal Control System Development Testing", ASME Paper 74-ENAs-43, dated 1 August 1974.

[7] Martinelli, R. C., et.al, "Isothermal Pressure Drop for Two-Phase Flow in a Horizontal Pipe", Trans. ASME, Feb. 1944, pp 139-151

[8] Griffith, P., "Two-Phase Flow in Pipes", Advances in Heat Transfer, MIT Press, 1963, pp 261-291.

[9] VSD Report T122RP09, "Development of a Refrigeration System for Lunar Surface and Spacecraft Application - Progress Report for the period of 1 September 1971 through 15 January 1972", dated 15 January 1972.

[10] Baker, O., "Design of Pipe Line for the Simultaneous Flow of Oil and Gas", The Oil and Gas Journal, July 26, 1954.

[11] Wiggins, C. L., "Dual-Mode Radiator/Zero-G Refrigeration System Test Report", VSD Report No. T122-RP-022, dated 1 May 1973.

[12] VSD Report No. T122-RP-015, Zero-G Radiator/Condenser Test Plan, 15 September 1972

[13] Wiggins, C. L., and J. L. Williams, "Quick-Look Test Report - Ground Test of Zero-G Condensation Experiment Apparatus", VSD Report No. T122-RP-017, dated 13 November 1972.

[14] Whitten, W. A., "Zero-G Radiator/Condenser Experiment Package Test", VSD Report No. T122-RP-020, dated 14 February 1973.

APPENDIX A

DEVELOPMENT OF A DIRECT CONDENSING RADIATOR FOR USE IN A SPACECRAFT VAPOR COMPRESSION REFRIGERATION SYSTEM

J. L. WILLIAMS
Senior Engineering Specialist,
LTV Aerospace Corp.,
Vought Systems Division,
Dallas, Texas

E. G. KESHOCK
Associate Professor,
Old Dominion University,
Norfolk, Va.

C. L. WIGGINS
Research Engineer,
Southwire Corp.,
Carrollton, Ga.

Development of a Direct Condensing Radiator for Use in a Spacecraft Vapor Compression Refrigeration System

The development and feasibility testing of a hybrid spacecraft heat rejection system that incorporates a single radiator capable of functioning as either a conventional space radiator or as a condenser in a refrigeration cycle is described. Emphasis is placed on development of the radiator condenser (RC), which is considered to be the most critical component of the hybrid system. The selection, design and fabrication of candidate RC configurations are described together with preliminary parametric analyses necessary to establish pressure drop, heat transfer and flow stability characteristics. Verification testing in one-g and zero-g environments is described, the latter condition being obtained by means of a C-135 aircraft. The testing included flow visualization (i.e., high-speed photography) of the condensation processes in a parallel channel quartz tube system modeling the RC. Representative qualitative photographs are presented. Results indicate stable flow conditions prevail for both one-g and zero-g operation.

Introduction

The objective of the present study was to develop a condensing space radiator for use in a spacecraft vapor compression refrigeration system. The present study was part of a program to develop a hybrid spacecraft heat rejection system with a single radiator that could function as either a conventional space radiator or as a condenser in a refrigeration cycle, thus the space radiator flow passages must be capable of accommodating either condensing two-phase flow or single-phase liquid flow.

The basic approach taken involved feasibility testing to demonstrate the operation of the hybrid heat rejection system, followed by development of individual components. The most critical component was considered to be the space radiator condenser (RC), which is the subject of this paper.

Development of the RC included (1) a requirements study to define the likely configuration of advanced spacecraft radiators, (2) parametric analyses of RC's to establish pressure drop, heat transfer, and flow stability characteristics, (3) selection and design of candidate configurations, (4) fabrication of candidate configurations, (5) design and fabrication of an experiment package for cinematography of condensing two-phase flow, and (6) verification testing in one-gravity and in zero-g while flying Keplerian trajectories in a C-135 aircraft.

Background

Refrigeration of the Environmental Control System (ECS) heat load in manned spacecraft has not been necessary to date. Expendable heat sinks such as water evaporators and conventional pumped fluid radiators have been entirely adequate. However, the following factors, either individually or collectively, may alter the presently satisfactory situation.

1 Construction of large space stations and other structures, coupled with clustering of many vehicles together (such as in docking a resupply vehicle into a space station) may dramatically reduce the accessibility of the excellent space heat sink at times.

2 Internal power requirements, and thus heat rejection requirements, may grow at a faster rate than surface availability for space radiators, particularly on reusable vehicles.

3 Imposition of contamination control constraints may preclude the use of water evaporators or like devices in the vicinity of astronomy or earth observation experiments.

In addition, future reduction in spacecraft power costs and the availability of a vapor compression machine in the vehicle, such as in reentry vehicles which have large cross-range capability, will tend to make refrigeration of spacecraft more attractive. Refrigeration systems become more attractive in spacecraft as the desired coolant outlet temperature approaches the equivalent radiator sink temperature, in which case the required space radiator area is dramatically increased. Usually the desired coolant temperature is 40 deg K, which is required in the dehumidification of cabin air, and possibly in the CO_2 removal process. If a regenerable life support system is used, the life support system process heat load requiring cooling to 40 deg F (278 deg K) is small compared to the total heat load. In addition, much of the electronic equipment which is cooled to 70–80 deg F (294–300 deg K) could be designed for higher temperature operation. Thus the vehicle heat load could be partitioned into low temperature (40 deg F) (278 deg K) and high temperature (~100 deg F (311 deg K)

Contributed by the Aerospace Division and presented at the Intersociety Conference on Environmental Systems, San Diego, Calif., July 16-19, 1973, of THE AMERICAN SOCIETY OF MECHANICAL ENGINEERS. Manuscript received at ASME Headquarters April 17, 1973. Paper No. 73-ENAs-5.

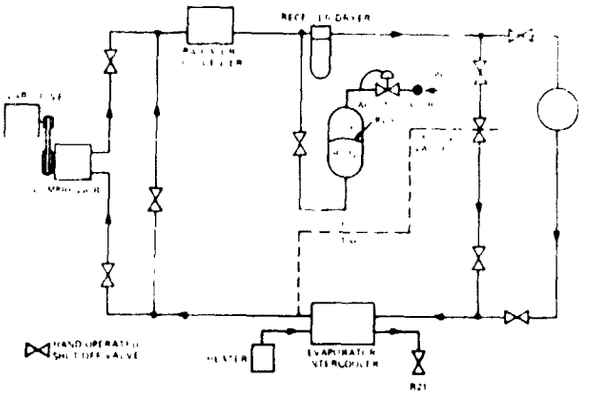

Fig. 1 Schematic of hybrid conventional radiator/vapor compression refrigeration system

sections, and the high temperature section would contain most of the load. For the space shuttle orbiter, the split could be 20-30 percent low temperature and 70-80 percent high temperature. Of course, a low temperature sink would almost always be available at some times for a spacecraft in earth orbit, and at those times the radiator could operate as a conventional pumped fluid system.

Hybrid System Development Program

Fig. 1 shows a schematic of the hybrid conventional radiator refrigeration cycle heat rejection system, as configured for the space shuttle orbiter. Unique development problems associated with this device include fluid inventory control and operating mode transfer procedures, in addition to the usual ones associated with two-phase flow in zero-g.

The mode transfer operation is crucial to the success of the system. During transfer from the liquid single-phase mode to the vapor compression mode, the compressor is used to force liquid out of the system into the accumulator. This operation requires that the compressor pump liquid for a short duration, thus the compressor may need a variable speed drive so that no damage will occur during the mode transfer operation. The relatively small portion of the heat load expected to be refrigerated (less than 30,000 BTU/hr [8.79 kW] for the shuttle orbiter), coupled with the necessity for high efficiency (to reduce power requirements) indicate the use of a positive displacement compressor. An efficient centrifugal compressor designed for the required heat load would have to operate at rotating speeds of above 100,000 rpm [1],[1] and it is unlikely that it could survive the liquid pumping operation without damage. In contrast, positive displacement compressors have little difficulty with liquid slugging, especially at low speed. Candidate compressors include (*a*) reciprocating, with reed valves, (*b*) rotary (or vane), with reed valves, (*c*) heli-rotor. The requirement for operation in zero-gravity will also affect the compressor selection. Generally, compressors used in terrestrial operations have gravity actuated lubrication systems. However, the rotary and heli-rotor compressors can be designed to obtain lubrication from the flowing refrigerant, either from oil suspended in the refrigerant, or from the refrigerant itself. Therefore, these compressors do not require gravity actuated lubrication systems, and, in fact, such compressors have been used in high performance aircraft which sustain adverse gravity environments for periods of 30-40 sec.

For feasibility testing to be conducted in a terrestrial environment compressor selection was made on the basis of low cost and availability, it was thought that some compressors might be damaged by liquid slugging as system operating techniques were perfected. The compressor selected was a Tecumseh Model 1100, which is normally used in automobile vapor cycle systems. It is a one-cylinder reciprocating compressor with reed valves. The compressor operated successfully through periodic intervals during a year of testing, including some 100 operating mode transfer operations, without degradation in overall system performance.

The refrigerant selection was related to the decision to use a mass produced (i.e., low cost) compressor, and so refrigerant 21 (R-12) was selected on the basis of lower vapor pressure than the other refrigerant (R-22) widely used in small positive displace-

[1] Numbers in brackets designate References at end of paper.

Nomenclature

A_L = cross-sectional area of liquid flow

$C_{L,g}$ = constant in empirical Martinelli equation for friction factor of liquid gas

D_c = maximum stable tube diameter

D_g = hydraulic diameter of gas flow

D_L = hydraulic diameter for liquid film

D_p = inside diameter of pipe

g = acceleration of gravity at sea level

g_c = conversion factor

G_L = liquid flowrate per unit area

G_T = total flowrate per unit area

G_v = vapor flowrate per unit area

h = heat transfer coefficient

k = thermal conductivity

l = arbitrary distance along the condensing length

L = length

L_c = condensing length

n = ratio of local acceleration of gravity to g_c

N_{We} = Weber number

P = pressure

Pr = Prandtl number

Re = Reynolds number for gas based on ω_g and D_p

Re_f = liquid-film Reynolds number

R = radius

t = thickness

T = temperature

U = liquid vapor interface velocity

W = fin width

X = vapor quality, G_v/G_T

X_{tt} = two-phase flow modulus for mechanism where both liquid and gas flow are turbulent

X_{tv} = two-phase flow modulus for mechanism where liquid flow is viscous and gas flow is turbulent

$\left(\frac{\Delta P}{\Delta l}\right)_{t,p}$ = pressure drop per unit length for two-phase flow

$\left(\frac{\Delta P}{\Delta L}\right)_g$ = pressure drop per unit length for gas flow

α = flow type modulus for liquid = $\frac{A_L}{\frac{\pi}{4} D_p^2}$

δ = liquid film thickness

Δ = incremental element

ϵ = emittance

θ = time

$\lambda = \left[\left(\frac{\rho_g}{0.075}\right)\left(\frac{\rho_L}{62.3}\right)\right]^{1/2}$ where ρ_g and ρ_L are in lb/ft^3

$\rho_{L,g}$ = liquid gas density

$\mu_{L,g}$ = liquid gas viscosity

σ = surface tension

ϕ_{tt} = function of X_{tt} used in calculation of pressure drop

ϕ_{tv} = function of X_{tv} used in calculation of pressure drop

$\omega_{L,g}$ = mass flowrate of liquid, gas

$\psi = \left(\frac{73}{\sigma}\right)\left[\mu_L\left(\frac{62.5}{\rho_L}\right)^2\right]^{1/3}$ where σ is in dyne/cm and ρ_L is in lb/ft^3

ment compressors. R-12 has not been used in conventional spacecraft radiator systems, principally because of a relatively low specific heat and a relatively high vapor pressure (as compared to RS89a, R-21, etc.). In modern spacecraft coolant selection, freezing temperature is one of the most significant parameters, and R-12 has an excellent freezing point of −252 deg F (115.5 deg K). Therefore, it could be used as the flight refrigerant coolant. R-21 has received wide attention as the coolant for future radiator systems [2, 3], and since rotary compressors are available for R-21, it could also be used as the refrigerant in a flight version of the hybrid conventional radiator refrigeration system. R-21 is an excellent refrigerant and has a 12 percent higher theoretical coefficient of performance (COP) than R-12 [4].

The accumulator also represents a major development item for the hybrid radiator refrigeration system. It must be capable of maintaining system pressure at a different level for each operating mode, and it must be capable of supplying or storing the refrigerant inventory difference between the two operating modes. A bladder-type tank pressurized from an external nitrogen supply was selected for the accumulator. A rejected NASA Scout Launch Vehicle attitude control system propellant tank and silastic bladder were initially used in the system testing. The bladder failed due to a flaw (which had caused it to be rejected on Scout), and was not replaced in subsequent testing in which gravity was used for separation of liquid and the pressurant gas.

A prototype zero-g evaporator (shown in Fig. 2) was used in the feasibility tests. It consists of a tube-in-tube heat exchanger, and has swirl fins in it. The evaporator picks up heat from a separate fluid loop which flows in the outer tube. This device is a "dry" evaporator, i.e., it has continuous flow as opposed to the "flooded" evaporator where the liquid refrigerant accumulates in a pool around the coil and boils off on demand. Refrigeration systems in high performance aircraft normally use "dry" evaporators. Controls for this system were not developed during this work; manual control of all system elements was generally used, the exception being that the constant superheat expansion valve was allowed to control evaporator outlet temperature during some test phases.

The bulk of the activity in this work was devoted to development of the condensing radiator, and the remainder of this paper is devoted to that effort.

Radiator/Condenser Design

An existing radiator design [2] was used as a preliminary model for the RC. Existing analytical techniques and experimental data were used as a basis for zero-gravity, two-phase flow design calculations.

After finalization of the RC design, two RC panels with tube diameters of 1.8-in. (3.18 mm) and 0.095-in. (2.4 mm), were fabricated and verification testing of the entire system was conducted under one-g conditions. The RC panel with 0.095-in. (2.4 mm) tubes was subsequently tested in a C-135 aircraft under simulated zero-g conditions. In addition, flow visualization tests of a model of the RC panel, involving high speed cinematography, were conducted under one-g and simulated zero-g conditions.

The design goals for the condenser radiator (RC) were:

a Have the same external dimensions as the individual shuttle orbiter radiator panels (6-ft (1.83m) wide by 12-ft (3.66m) in length).

b Operate at a maximum condensing temperature of 150 deg F (338.9 deg K).

c Reject up to 9000 BTU/hr (2.637 kW) to a sink temperature of 0 deg F (273.1 deg K).

d Use constant area parallel flow passages of about 1.8 in. (4.5 mm) I.D. [2].

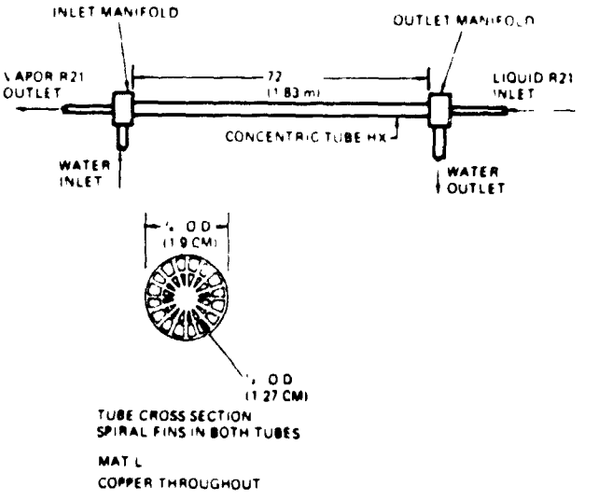

Fig. 2 Evaporator/intercooler design

e Have a flowrate of at least 40 lb/hr-tube (5.04 g/s-tube) in the all-liquid operating mode (sufficient to provide turbulent flow).

f Incur a maximum RC pressure drop of 5 psi (35 kPa) in the all-liquid mode at 14 psi (28 kPa) in the vapor-cycle mode.

g Maintain hydrodynamically stable flow in the RC in the vapor-cycle mode, such that no vapor is introduced into the RC outlet manifold.

h Provide positive liquid collection at the outlet header.

i Operate successfully with an acceleration of 0.1-g along any axis of the radiator.

Satisfaction of these design goals was believed necessary to yield a heat rejection system which could easily be integrated into current or advanced spacecraft.

Two-Phase Flow Stability. There has been considerable investigation of condensing two-phase flow stability, in one-g, and some also in zero-g fields. Several types of two-phase flow can exist in tubes, examples of which are shown in Fig. 3. Literature surveyed indicated that annular flow is the most stable two-phase flow regime for a wetting fluid. The terms "wetting" and "nonwetting" refer to the action of a liquid on a surface. For example, liquid mercury tends to ball-up on aluminum, so it is a "nonwetting" fluid. R-12 tends to spread out so it is a wetting fluid. Basically, stability, in the context of RC operation, means that the flow regime patterns along the length of the tubes are constant with time. Such behavior tends to prevent large inventory changes in the RC, which would affect the operation of the system since overall inventory is fixed for each operating mode. It also tends to prevent large pressure fluctuations, and finally oscillation of the liquid leg of the tubes is avoided. If oscillation occurs it could result in vapor passing into the liquid header, or plugging of the tube by liquid backing into the vapor header. Broadly speaking, the condition of stability is achieved if perturbations to the system are damped out rather than being amplified. The most significant types of annular flow instabilities are interfacial instability at the vapor/liquid interface and film or hydrodynamic instability.

The classic form for annular condensing flow is shown in Fig. 4. The liquid film remains relatively thin, and has increasing velocity in the direction of flow, while the vapor velocity decreases as the vapor mass flow rate decreases more rapidly than the vapor flow area. Eventually the vapor velocity becomes zero where all the vapor is condensed. At this point the liquid velocity is quite low since it now occupies the entire flow channel

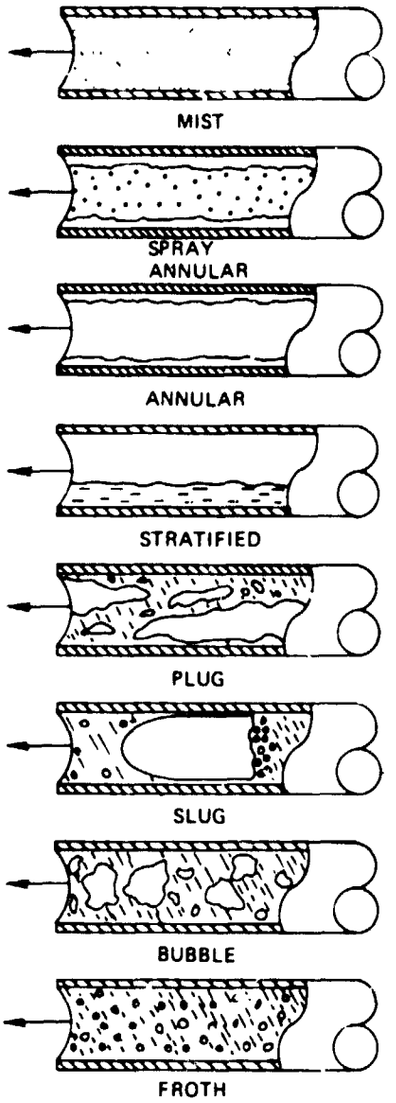

Fig. 3 Two-phase flow patterns

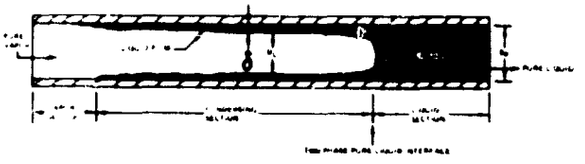

Fig. 4 Condensation with a stable annular flow pattern

This liquid velocity decline is accompanied by a static pressure increase, due to the change in momentum. Interfacial or Taylor instability can occur at this point when gravity causes the interface to collapse, allowing vapor to proceed beyond the interface location. This type of instability is obviously a function of the tube diameter and the local acceleration field. Dennington [8] has defined the maximum stable tube diameter as

$$D_s \leq 1.835 \left[\frac{\sigma}{(\rho_L - \rho_v)g} \right]^{1/2} \quad (1)$$

Surface tension (σ) and density (ρ) are properties of the particular fluid, and are a function of temperature. Fig. 5 shows the

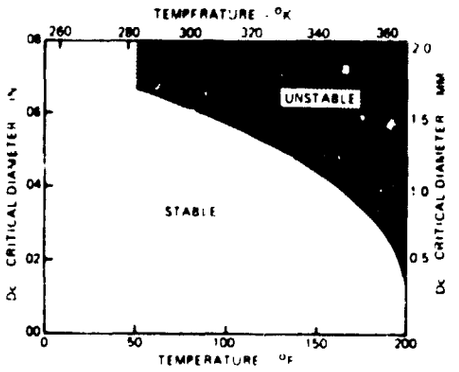

Fig. 5 Critical stable diameter versus condensing temperature for refrigerant 12 in a one-g field

critical diameter for R-12 as a function of temperature. For an operating temperature of 150 deg F (338.9 deg K) the critical diameter in a one-g field is 0.045-in. (1.14 mm), while in a zero-g field it is infinite. There are numerous types of film or hydrodynamic instability, such as:

1 Tollmien-Schlichting, which is a result of viscosity amplification of disturbances occurring when the liquid film undergoes transition from laminar to turbulent flow [5, 6]

2 Kelvin-Helmholtz, which results from interaction between the vapor and liquid films in the form of aerodynamic pressure which tends to lift the liquid [7]

3 Gravity runback, which occurs when an acceleration force along the axis of the tube opposite to the direction of flow causes the liquid film to flow back against the vapor flow

The biggest factor leading to liquid film bridging and development of slug flow appears to be the Kelvin-Helmholtz instability [7]. Miles [9] has developed a two-phase flow stability criterion which may be expressed in the form of the liquid film Reynolds number and the Weber number at the liquid surface. Basing the liquid Reynolds number on free surface velocity and film depth, Miles determined that for large liquid Reynolds numbers, i.e., $Re_L \to \infty$, a sufficient condition for stability is that the Weber number be less than 3. As a lower bound, he found that there exists a critical liquid Reynolds number below which the flow will always be stable. His calculations indicate that the value of this Reynolds number is approximately 200. These two stability criteria are calculated as follows

$$N_W = \frac{\rho_L \cdot u_i^2 \cdot \delta}{g_c \, \sigma} \leq 3 \text{ for stability} \quad (2)$$

$$Re_L = \frac{\rho_L \, u_i \, \delta}{\mu_L} \leq 200 \text{ for stability} \quad (3)$$

It can be seen from equations (2) and (3) that the criteria for hydrodynamic stability during annular flow may be determined by calculating liquid free surface velocity and film thickness. Since these parameters change over the entire length of the condenser tube, the Weber and liquid film Reynolds number must be evaluated over the entire tube length.

This criterion was applied to the present design for a flowrate of 20 lb/hr (2.52 g/s), which represents the flow at the maximum heat load in the vapor-cycle mode, with the results shown in Fig. 6. These results indicate that a 3/8-in. (9.53 mm) I.D. tube is required for stability over all liquid-film Reynolds numbers expected for a 12-ft (3.66 m) tube. The maximum liquid Reynolds number approaches 2000, so increasingly smaller diameter tubes would tend to produce instability prior to complete condensation. These results tend to show that stability cannot be achieved with the desired tube diameter of 1/8-in. (3.18

mm). This small diameter is desirable because it; (*a*) is the optimum diameter for conventional radiator operation; (*b*) favors system operating stability because of a smaller fluid inventory in the condenser; and (*c*) requires a smaller accumulator for the operating mode changeover, since the fluid inventory is smaller. For these reasons, the flow regime for the 1/8-in. (3.18 mm) tube was explored further.

The approach used to predict the flow regimes expected within the condenser tubes was based upon the experiments of Baker [10]. His results are presented in the form of a flow regime map, shown in Fig. 6, and are based upon adiabatic two-component, two-phase flow. Since two-component, two-phase flow results have frequently proved to be applicable to single component, two-phase flow systems, it was considered that use of Baker's flow-regime map was justifiable. This method is based on the parameters:

$$\lambda = \left[\left(\frac{\rho_g}{0.075}\right)\left(\frac{\rho_L}{62.3}\right)\right]^{1/2} \tag{4}$$

$$\psi = \left(\frac{73}{\sigma}\right)\left[\mu_L\left(\frac{62.3}{\rho_L}\right)^2\right]^{1/3} \tag{5}$$

and plots of G_v/λ versus $G_L\lambda\psi/G_v$. Fig. 7 shows a Baker Chart with various flowrates for a 1/8-in. (3.18 mm) tube plotted on it. in the condensing flow case $G_v = f(G_L)$, and if it is assumed that quality varies linearly along the condensing length, then since

$$G_T = G_v + G_L \tag{6}$$

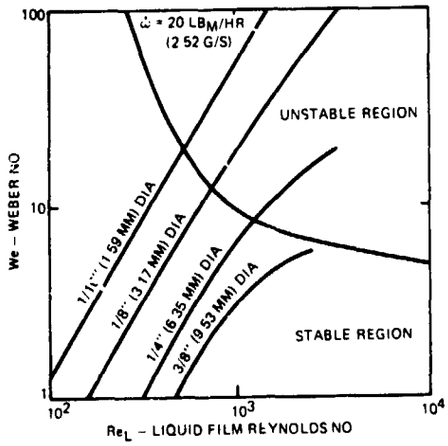

Fig. 6 Hydrodynamic stability criteria

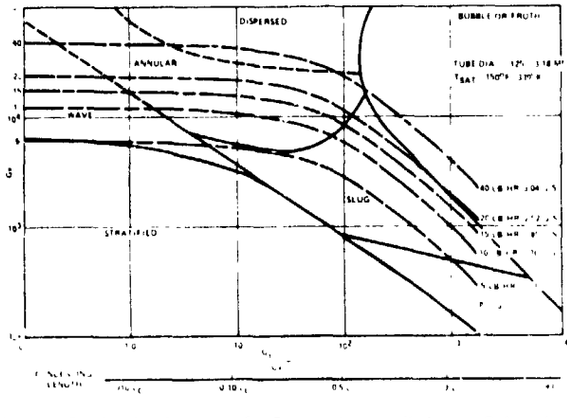

Fig. 7 Condensing heat transfer flow regime prediction on Baker chart

$$X = \frac{G_v}{G_T} \tag{7}$$

and

$$X \cong l/L_c \tag{8}$$

it is possible to solve for G_L/G_v as a function of L_c by combining equations (6), (7), and (8)

$$\frac{G_L}{G_v} \cong \frac{L_c - l}{l} \tag{9}$$

This then defines L_c as a function of G_v/λ. This function is shown on Fig. 7, and it indicates that for a 1/8-in. (3.18 mm) diameter tube, a transition to slug flow will occur at about 1/2 of the condensing length, and that plug flow will occur at about 0.9 of the condensing length.

Thus, these analytical results indicate that annular flow will not exist down the entire length of the condensing section. Possibly as a result of similar analyses, many authors [6, 8, 16, and 17] have suggested that tapered tubes are necessary to produce stable flow in zero-g condensation. They reason that reducing tube diameter in the direction of the flow increases the vapor velocity, thus helping prevent bridging of liquid across the tube. It has also been suggested [6] that the use of orifices in each tube at the liquid manifold would produce a more stable flow. These approaches were demonstrated to have merit by Soliman [6]. However, in the present work the tapered tube was judged too difficult to produce, and introduction of orifices was found to increase the pressure drop appreciably

It is possible for stable slug flow to exist, of course [11]. This seems to be a particularly reasonable expectation for small diameter tubes, where capillary action is significant. Work done on slug flow by Suo [12, 13] indicates that stable transition to slug flow occurs in capillary tubes, and based on criteria given in that work, the flow in low quality regions of the tubes presently under consideration should be in a region of dominant capillary action, particularly when under zero-gravity conditions. On this basis it was decided to use straight tubes with no orifices for the initial testing, and to resort to the use of orifices only if it were demonstrated that stable flow could not be achieved without them.

Pressure Drop Computations. Accurate prediction of two-phase flow pressure drop in tubes is extremely difficult, and requires knowledge of the flow regime along the entire tube. However, the most widely used technique for predicting two-phase flow in tubes is that of Martinelli [14], which assumes that the pressure drop of the separate liquid and gas phases are equal, and makes no assumption regarding the specific flow configuration. Martinelli's predictions assume that the flow is steady and that an annular, dispersed flow pattern exists [15]. A computer routine which calculates a steady-state flow and thermal balance on a single RC tube was developed for use in RC panel design. This routine is described briefly in Appendix A. It uses a modified version of the Martinelli approach (described in Appendix B) to compute the two-phase flow pressure drop in the tube. The liquid film thickness is computed from the Martinelli correlation for annular flow as described in Appendix B. Two-phase flow stability parameters are also computed in this routine. Total tube pressure drop is calculated by use of Darcy equation for the single phase regions.

Results of the pressure drop analysis are shown in Fig. 8. These results indicate that the 1/8-in. (3.18 mm) and larger tubes yield a pressure drop which is within the required range of less than 4 psi (28 kPa).

Heat Transfer. As described in Appendix A, the computer routine calculated steady-state heat transfer for small elements of the tube in sequence along the entire tube length. The familiar Dittus-Boelter equation was used for determination of heat trans-

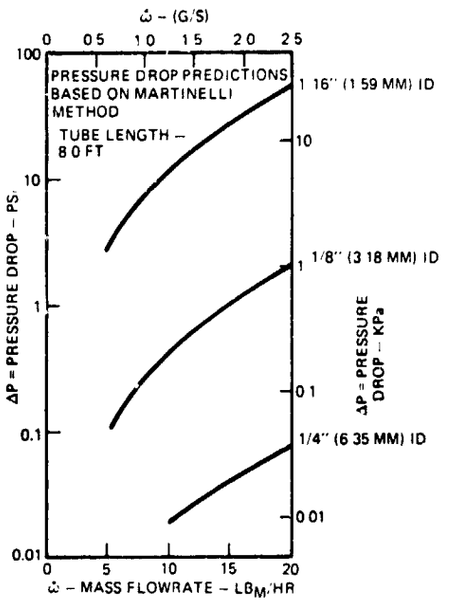

Fig. 8 Radiator/condenser pressure drop versus flow rate

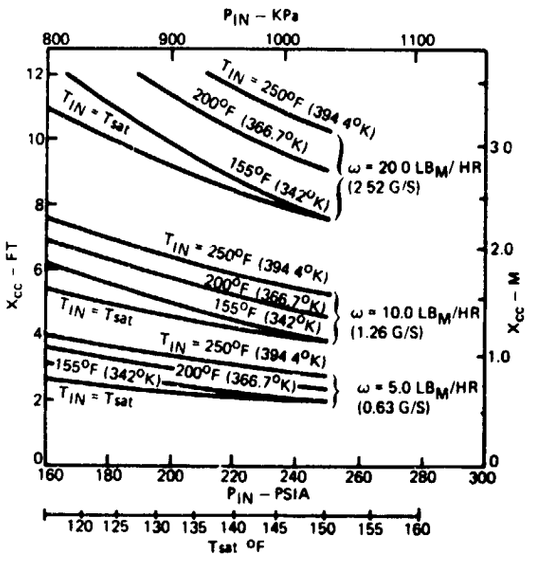

Fig. 9 Condensing length required for various inlet temperature and pressure conditions

fer coefficients in the turbulent single-phase flow regions of the tube (Re > 2000)

$$h = 0.023 \left(\frac{k}{D_p}\right) \mathrm{Re}^{0.8} \mathrm{P_r}^{0.3} \tag{10}$$

and

$$h = 3.66 \frac{k}{D} \tag{11}$$

was used for laminar flow (Re ≤ 2000)

Several techniques are available for calculating the heat transfer coefficient in condensing flow [18–20]. However good agreement was not found among these approaches. In this case, the condensing heat transfer (hA) term is one or two orders of magnitude greater than the radiation (UA) term, so great accuracy in the condensing heat transfer coefficient is not required. The method of Akers and Rosson [9] was selected for use in this work, primarily because it was available in coded form from another computer routine.

It was planned to design for a minimum area radiator, rather than a minimum weight radiator, so radiator fin efficiencies of 0.9 [24] were considered. For the 0.063-in. (1.6 mm) thick aluminum plate selected for the radiator (on the basis of ease of fabrication) this resulted in an 8-in. (20.3 mm) tube spacing. For the 72-in. (1.83m) wide panel, this results in 9 parallel flow paths. The radiators were coated with 3M Black Velvet Paint, which was assumed to have an emittance, ϵ, of 0.9.

Results from the routine are given in Fig. 9, where required condenser tube length is plotted against inlet saturation pressure (and temperature) with inlet temperature as a parameter for various flowrates. These results show that a 12-ft (3.66 m) tube will provide complete condensation for a flowrate of 20 lb/hr-tube (2.52 g/s-tube) in a 1/8-in. (3.18 mm) tube with an inlet pressure of 220 psi (1517 kPa) and an inlet temperature of 250 deg F (394.4 deg K). The results also show that the required tube length increases with increasing inlet temperature, and decreases with increasing inlet pressure (that is, with increasing saturation temperature).

Radiator/Condenser Panel Design. Based on the foregoing analysis the radiator configuration shown in Fig. 10 was evolved. It was decided to test two RC panels with different diameter tubes. Both RC panels were made from 0.063-in. (1.6 mm) thick 5052 Al sheet, with extruded 6063 Al tubes. The tube diameters were 1/8-in. (3.18 mm) I.D. and 0.095-in. (2.4 mm) I.D. of configurations shown in Fig. 10. A 1-in. (2.54 cm) I.D. gas header and a 1/2-in. (1.27 cm) I.D. liquid header were used on both radiators.

Test Program

Three series of tests have been conducted and a fourth is planned. The first tests involved the complete hybrid radiator/refrigeration system in a space environment simulator (SES).

Hybrid Radiator Refrigeration System Testing. Fig. 11 shows the test set-up with the two radiator panels mounted back-to-back in the SES. The panels were tested sequentially and each was tested in the radiator and the vapor cycle modes. There were also numerous mode transfer operations made during the course of the test.

Fig. 12 compares measured and predicted RC panel temperatures along the length of the panel for two flowrates. These results are typical and demonstrate the general good agreement between predicted and measured results that was obtained. The knee in these curves indicates the point where condensation is complete. The point of ocmplete condensation is about the

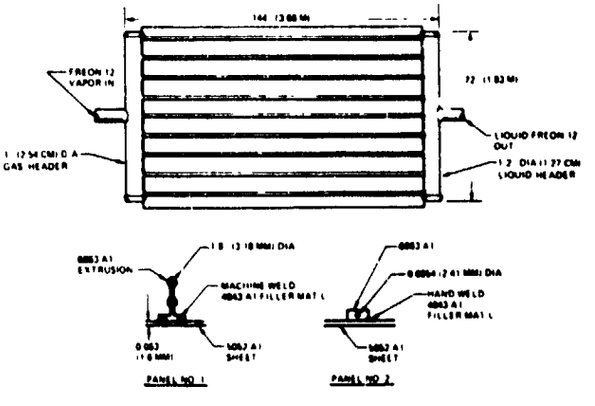

Fig. 10 Radiator/condenser design

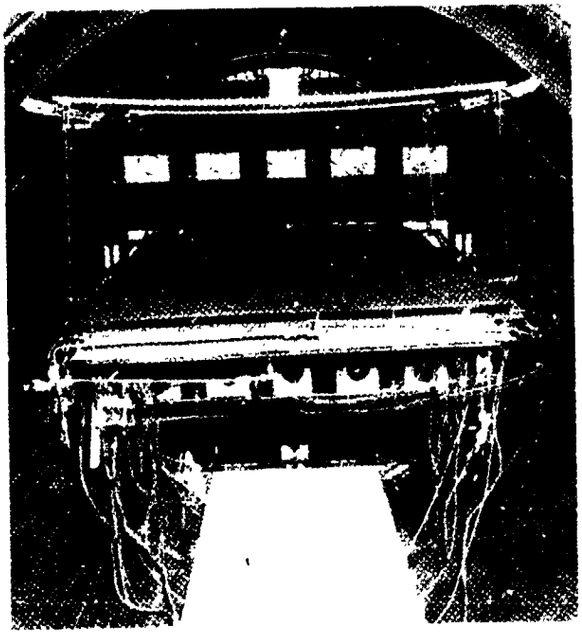

Fig. 11 Radiator/condenser panels mounted in space environment simulator

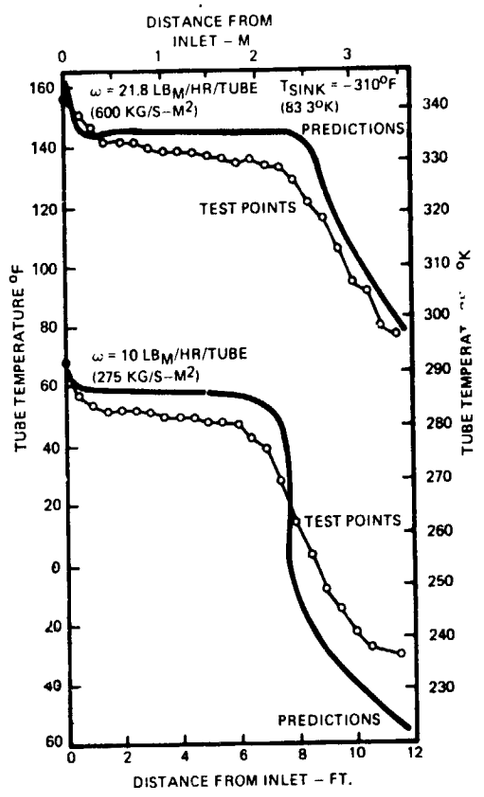

Fig. 12 Comparison of predicted and measured radiator/condenser panel temperature profiles

same in both predictions and data; however, the data do not show as abrupt a change in temperature as the analysis. The analysis is undoubtedly weak in the transition region, since it assumes annular flow throughout the entire two-phase flow region. Predictions of flow regime, however, indicate that slug flow develops, but there is no suitable heat transfer correlation available for this region.

Pressure drop predictions are compared with test data in Table 1 These results are especially good since prediction of two-phase flow pressure drop is usually only accurate to about 60 percent [15]. In this case not only was the two-phase flow pressure drop predicted, but also the two-phase flow length was included in the prediction. The predictions are consistently high, and this may be due to the flow regime model used in the analysis which considered annular flow to the transition point. If this is true, then the liquid bubble type flow may have a lower pressure drop than annular flow. In any event, the Martinelli assumption of equal pressure drops for each phase is not true for plug or large bubble type flow.

Another element of the test involved elevation and depression of the outlet of the panel to simulate 0.1-g acceleration along the axis of the radiator. No flow instability was evident from this test. Against the adverse gravity, the condenser pressure increased and the condensing length decreased, corresponding to a longer liquid leg, while in the downward flow case, the condenser pressure decreased and the liquid leg was shorter.

Flow Visualization and Zero-g Testing. The SES tests yielded good system performance data; but it was difficult to obtain insight into the nature of the two-phase condensing flow with the resulting temperature and pressure drop data. The most direct method of obtaining this insight is by visualization of the flow, and use of very high speed photography to slow the action to a point where it can be observed. Visualization allows positive identification of the flow regime encountered. It also clearly shows if there are any gross instabilities, such as oscillation of the liquid leg or similar phenomena. In addition, it provides data on liquid surface wave frequency and amplification which can be used to upgrade instability theories. Also, data under zero-g conditions were desirable to provide confidence that the RC panel would perform as expected.

For these reasons, a test program involving simulated zero-gravity conditions produced by a C-135 aircraft flying trajectories such as shown in Fig. 13 was initiated. This type of simulation produces a low-acceleration field for 15 to 20 sec, and has been used extensively by Namkoong and others in studies of

Table 1 Pressure drop test data comparison with predictions

TUBE DIA		P_{IN}		T_{IN}		FLOW RATE PER TUBE		PREDICTED ΔP_P		MEASURED ΔP_M		DEVIATION% $\frac{100(\Delta P_P - \Delta P_M)}{\Delta P_M}$
INCH	(MM)	PSIG	KPa	°F	°K	(LB/HR)	(G/S)	PSI	KPa	PSI	KPa	
1/8	3.175	187	1263	126	325.6	21.4	2.69	2.9	20	2.8	19.3	1.6
1/8	3.175	152	1150	118	321.1	20.0	2.52	2.9	20	2.5	17.2	16.0
1/8	3.175	[illegible]	1287	178	354.4	18.2	2.29	2.1	14.5	1.7	11.7	23.4
1/8	3.175	123	860	162	340	16.9	2.13	2.1	14.5	1.7	11.7	23.4
1/8	3.126	206	1515	181	356.1	23.1	2.91	2.8	19.3	2.4	16.5	16.7
0.086	2.413	237	1736	186	358.3	25.4	3.2	11.5	79.3	8.4	57.9	37.0
0.086	2.413	240	1786	150	338.9	26.7	3.36	10.4	71.7	8.0	61.4	16.8
0.086	2.413	188	1290	167	342.8	20.0	2.52	10.1	69.6	7.0	48.3	43.1
0.086	2.413	193	1432	162	340	20.0	2.52	8.5	58.6	8.4	57.9	1.2
0.086	2.413	134	1026	132	328.9	16.7	2.10	7.4	51	7.2	49.6	2.8
AVERAGE												18.4
MEAN												16.7
STD DEVIATION												13.4

nonwetting flow for use in design of spacecraft power plant RC panels [21–23].

The time interval for establishment of any change in conditions is short, but this should be sufficient for any hydrodynamic changes to the flow From Dennington [8], the time for a surface in a tube to obtain a new equilibrium shape when it moves into zero-gravity is

$$\theta = L\frac{R\rho_L}{2\sigma g_c} \tag{12}$$

Thus, according to equation (12), the time required for the surface in a 1/8-in. (3.18 mm) ID tube to move 6-in. (15.24 cm) is 0.66 sec.

The time for establishment of new equilibrium thermal conditions is less well defined, but the change in thermal conditions was believed to be of such small magnitude as to have only a second order effect on the flow pattern.

The flow visualization experiment was designed as shown schematically in Fig. 14. R-12 is stored in a tank which can be heated to provide the desired system pressure. Liquid R-12 is withdrawn from the tank and put through an electric heater where it is raised to the desired temperature level. The R-12 then flows to a gas receiver which damps out any pressure fluctuations caused by flashing in the heater. It then flows into a heater with three parallel tubes made of fused quartz, down the

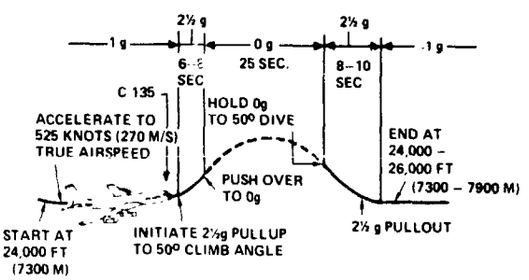

Fig. 13 Aircraft zero gravity maneuver

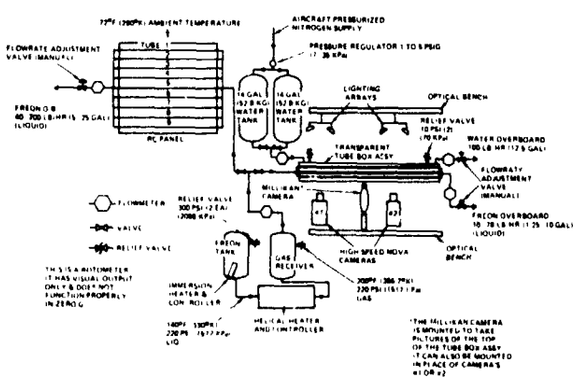

Fig. 14 Test apparatus flow schematic

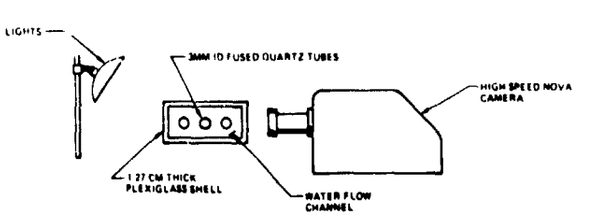

Fig. 15 Flow passage arrangement

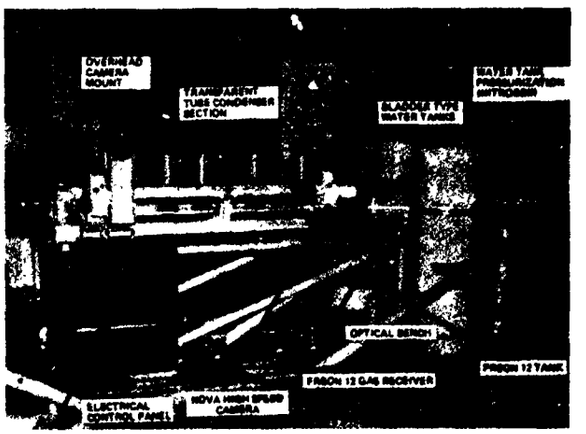

Fig. 16 Zero-g condensation experiment apparatus

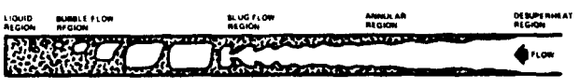

Fig. 17 Sketch depicting typical map of condensing two-phase flow regimes observed

8-ft (2.44 m) length of the tubes, and then overboard. The cooling medium is water which is stored in two bladder tanks pressurized by aircraft nitrogen supply. The water flows in parallel with the R-12 in a channel comprised of 1/2-in. (1.27 cm) thick plexiglass, as shown in Fig. 15.

The complete experiment package is shown in Fig. 16. The high speed cameras are mounted on optical benches which permit them to be moved along the axis of the tubes. Two cameras take motion pictures of the outside R-12 tubes, while a third camera photographs all three tubes from above. The flow passages and the optical benches are shock mounted to damp out all vibrations above a frequency of 12 Hz.

As indicated in Fig. 14, the RC panel with 0.095-in. (2.4 mm) ID flow passages was also included in the aircraft testing. It was instrumented with 27 thermocouples, 4 absolute pressure transducers, and 5 pressure drop transducers. Heat was rejected from it to the cabin atmosphere and surroundings.

The visualization experiment indicates that the two-phase flow regimes down the tube are as shown in Fig. 17. There is a considerable amount of wave action on the liquid film from the earliest observable point. The flow gradually develops large waves which eventually bridge the tube and isolate large vapor bubbles. These bubbles flow rather steadily down the tube, while growing steadily smaller until they are finally extinguished. This same flow pattern prevails over most of the range tested, that is, from 5 lb/hr-tube (0.63 g/s-tube) to 20 lb/hr-tube (2.52 g/s-tube). At 5 lb/hr-tube (0.63 g/s-tube) it appears that the flow is initially stratified, rather than being annular.

The flow is steady in appearance, and there is no sharp boundary between the condensing region and the pure liquid region. Only minor oscillations of the liquid leg were observed. The fluid inventory in the tube gives every indication of being remarkably constant.

The pressure instrumentation in the tests conducted so far has been quite erratic, but it appears that there are no significant pressure fluctuations. During the portion of this test where the outlet end of the tubes were raised to represent an adverse pressure gradient, the liquid leg length increased by 100 percent. However, the pressure instrumentation was not operative at this time, so pressure changes could not be recorded. High-speed photography of the flow indicates it is not substantially affected by the adverse gravity gradient.

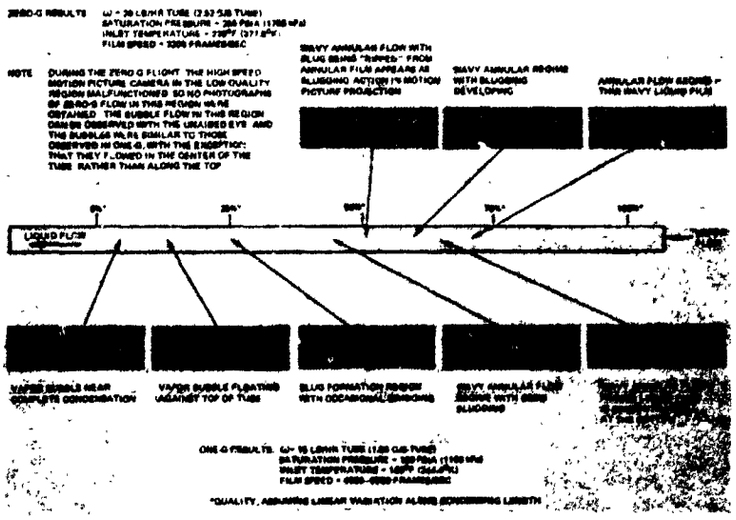

Fig. 18 Photographs of one-g and zero-g flow

Fig. 18 shows a sequence of photographs of the flow at different stations along the tube; the photographs were not taken at the same time, but are at essentially the same conditions. This sequence illustrates typical flow conditions observed in one-g, and in zero-g.

In zero-g the flow appears to be more annular in nature than in one-g, with a noticeably smaller liquid film on the bottom of the tube. Bubbles in the flow tend to be centered in the tube, rather than riding along the top of the tube as they do in 1-g. Also, the length required for condensation appears somewhat shorter than in the one-g condition. Additionally the flow has the same stable character in zero-g as was observed in one-g.

Conclusions

The primary conclusions reached in this study were that a hydrodynamically stable RC can be designed for operation with a spacecraft refrigeration system, and that a hybrid conventional radiator/vapor cycle heat rejection system is feasible.

Acknowledgments

This work was sponsored by NASA-Johnson Spaceflight Center (JSC) under Contract NAS9-12055, with Mr. Burrell French as the Technical Monitor.

The authors gratefully acknowledge the help of Mr. H. R. Howell, who conducted the hybrid system feasibility tests, Mr. Dave Baskett, who designed and supervised construction of the hybrid system test, and Mr. Jim Gilchrist who designed and supervised fabrication and checkout of the zero-g experiment package.

In addition the authors acknowledge the efforts of Mr. Taylor Moorman of NASA-JSC, who was responsible for the high speed photography and Messrs. Gordon Spencer of NASA-JSC and Don Griggs of Wright-Patterson Air Force Base, who assisted in conducting tests on the simulated zero-g flights.

APPENDIX A

Condensing Radiator Analysis Computer Routine

A computer routine was written for the purpose of analyzing condensing two-phase flow in a space radiator. The routine provides a steady-state solution, which is generated by doing successive steady-state heat transfer analyses on small elements along the length of a single tube of the radiator starting at the inlet as shown in Fig. 19. It is assumed that there is an adiabatic mid-point in the fin between the tubes, and that all tubes are in a similar environment. This appendix describes the computer routine very briefly.

Input Data

- Inlet fluid flow conditions
  - Temperature
  - Pressure
  - Flowrate
- Environmental conditions
  - Sink temperature, T_s
  - Fin surface emittance, ϵ
- Radiator geometry
  - Internal flow passage diameter, D
  - Fin thickness, t
  - Fin width, W
  - Tube length, L (The routine will continue to increment length until condensation is complete if a zero is input for length)
- Computation parameter
  - Element length, ΔL (Normally 0.01 ft [3 mm] was used)
  - Output frequency along tube length (usually 6-in. [15.24 cm] or 1 ft [30.48 cm] was used)

Internal Computations

The routine was specificially set up for refrigerant 12, and it calculated all required fluid properties such as saturation pressure, viscosity, surface tension, etc., at the required temperature.

The sequence of computations was as follows:

(*a*) Physical properties of fluid based on element inlet conditions.

(*b*) Heat transfer coefficient based on the method of Akers and Rosson [19]. It was considered to be reasonable to start with the heat transfer coefficient and to not iterate by re-computing heat transfer coefficient after liquid film thickness is established, because the fin radiation heat transfer dominates the heat transfer process. Large changes in the fluid heat transfer coefficient have little effect on the overall heat transfer rate.

(*c*) Heat transfer from the fin, and steady state temperatures are computed.

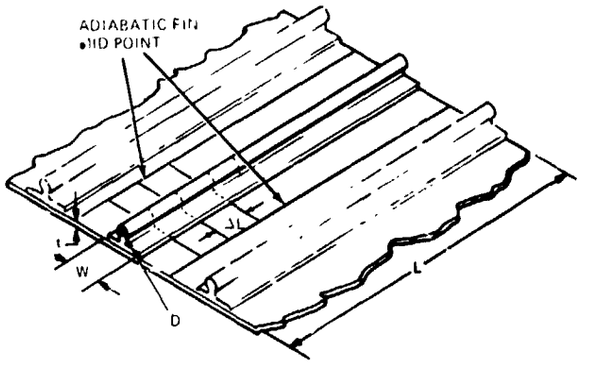

Fig. 19 Radiator/condenser analytical model

(*d*) If the fluid temperature drop puts it below the saturation temperature, the fluid temperature is set at the saturation temperature, and mass transfer from the vapor to the liquid state is calculated.

(*e*) Pressure drop is computed using the Darcy equation in single-phase flow, or using the modified Martinelli approach described in Appendix B for two-phase flow. Liquid film thickness in two-phase flow is calculated as described in Appendix B.

(*f*) Liquid film Reynolds number and Weber number are computed.

(*g*) Steps *a* through *f* are repeated for each element of the tube in sequence.

(*h*) The total radiator pressure drop is computed.

Output Data

Results are output at specified locations along the tube length as follows:

Fluid temperature
Tube temperature
Liquid film thickness
Gas Reynolds number
Liquid Reynolds number
Liquid Weber number
Gas flowrate
Liquid flowrate
Incremental pressure drop

In addition, the following are output for the tubes:

Outlet temperature
Outlet pressure
Total pressure drop
Condensation length

APPENDIX B

Modified Martinelli Method for Calculation of Two-Phase Flow Pressure Drop and Liquid-Film Thickness

Prediction of pressure drop for two-phase condensing flow in a space radiator requires a suitable analytical model of the flow. When two phases flow concurrently in a tube they can assume many complex flow patterns, as shown on Fig. 3. To accurately predict two-phase flow pressure drop, mathematical models based on a particular flow pattern are required, since no single correlation or mathematical model can cover all possible flow patterns. Due to the complexities involved in a purely mathematical analysis, experimentation is used to obtain solutions. A well known correlation was developed by Martinelli [14], in which the pressure drop of each phase was considered equal, and correlating parameters were derived from relations governing the pressure drop of each of the phases as if it were flowing alone. The correlation assumes that an annular dispersed flow pattern exists, with no knowledge of other flow configuration details being required

The key to the approach is the identification of a flow modulus, α, which accounts for the geometry of the flow, as well as relative motion or slip effects between the liquid film and the gas core. The flow modulus can be defined as

$$\alpha = \frac{A_L}{\frac{\pi}{4} D_L^2} \tag{13}$$

However, the quantities A_L and D_L cannot be directly determined, in general.

In this study, a stability evaluation of the two-phase flow was desired, and this required a knowledge of the liquid film thickness. The most stable flow pattern, and thus the most desirable, was annular flow. If the annular flow were stable, then, in a zero-gravity environment, it is possible to express α in terms of the liquid film thickness, δ. This is because δ is the same all around the tube periphery, which it would not be in one-g, or if the flow were less stable.

The method for calculating pressure drop and film thickness is developed as follows from reference [14]:

$$\left(\frac{\Delta P}{\Delta L}\right)_{T-P} = \left(\frac{\Delta P}{\Delta L}\right)_g \left(\frac{D_P}{D_g}\right)^{4.8} \tag{14}$$

For turbulent gas and turbulent liquid

$$\left(\frac{D_P}{D_g}\right)^{4.8} = \Phi_{tt}^2 = (1 + \alpha^{1/4} \cdot X_{tt}^{2/4})^{2.4} \tag{15}$$

For viscous liquid and turbulent gas

$$\left(\frac{D_P}{D_g}\right)^{4.8} = \Phi_{vt}^2 = (1 + \alpha^{1/2} \cdot X_{vt}^{1/2})^2 \tag{16}$$

where

$$X_{tt} = \left(\frac{\mu_L}{\mu_g}\right)^{0.111} \left(\frac{\rho_g}{\rho_L}\right)^{0.555} \left(\frac{\dot{\omega}_L}{\dot{\omega}_g}\right) \tag{17}$$

$$X_{vt} = \frac{C_L}{C_g} (\mathrm{Re}_g)^{-0.8} \frac{\rho_g}{\rho_L} \frac{\mu_L}{\mu_g} \frac{W_L}{W_g} \tag{18}$$

In this study the gas was always turbulent (i.e., Re > 2000), and the liquid transition Reynolds number was 1000.

For the assumed perfect annular flow

$$D_L = 2\delta \tag{19}$$

$$D_g = D_P - 2\delta \tag{20}$$

$$\alpha = \frac{D_P - \delta}{\delta} \tag{21}$$

$$\frac{D_P}{D_g} = \frac{\alpha + 1}{\alpha - 1} \tag{22}$$

Substituting equation (22) into equation (15)

$$\left(\frac{\alpha + 1}{\alpha - 1}\right)^{4.8} = (1 + \alpha^{1/4} \cdot X_{tt}^{2/4})^{2.4} \tag{23}$$

which reduces to

$$X_{tt} = \frac{6.35}{(\alpha - 1)^{1.0667}} \tag{24}$$

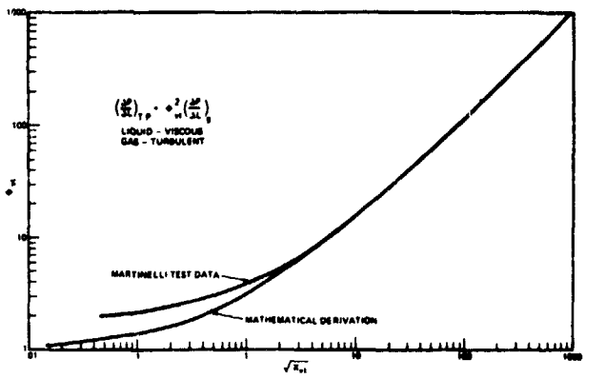

Fig. 20 Modulus Φ_{vt} versus two-phase flow modulus $\sqrt{X_{tt}}$

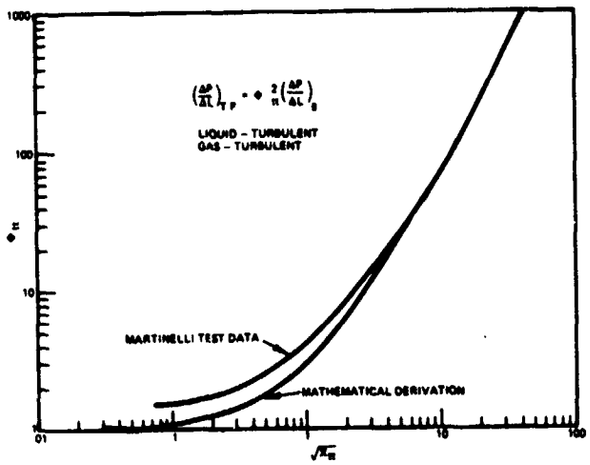

Fig. 21 Modulus Φ_{tt} versus two-phase flow modulus $\sqrt{X_{tt}}$

By equating equations (17) and (24), it is possible to solve for α directly. Then equation (21) can be solved for δ, and equation (15) can be solved for ϕ_{tt}^2, which permits computation of two phase pressure drop with equation (14).

A similar procedure can be used on the viscous-turbulent flow to yield

$$X_{vt} = \frac{\left[\left(\frac{\alpha+1}{\alpha-1}\right)^{2.4} - 1.0\right]^2}{\alpha} \tag{25}$$

This approach gives the film modulus α as a function of X_{tt} and X_{vt} without benefit of experiment. However, it is prudent to check the result to see how well it correlates with experimental data. Figs. 20 and 21 show comparisons of the computed and experimental values of ϕ_{vt} and ϕ_{tt}, respectively. Fig. 22 shows the computed pressure drop for the modified Martinelli, and the original Martinelli correlations. As can be seen, the original Martinelli correlation gives pressure drops 12–15 percent higher than the modified version.

As discussed in the text, the stability analyses predicated upon this model indicated that an unstable liquid/vapor interface would always occur, so the perfect annular flow model was never valid. This was verified by the zero-g experiments, in which perfect annular flow did not exist down the entire length of the tube, but rather slug flow developed. Nevertheless, the predicted pressure drops with this approach were consistently more accurate than with the original Martinelli correlation.

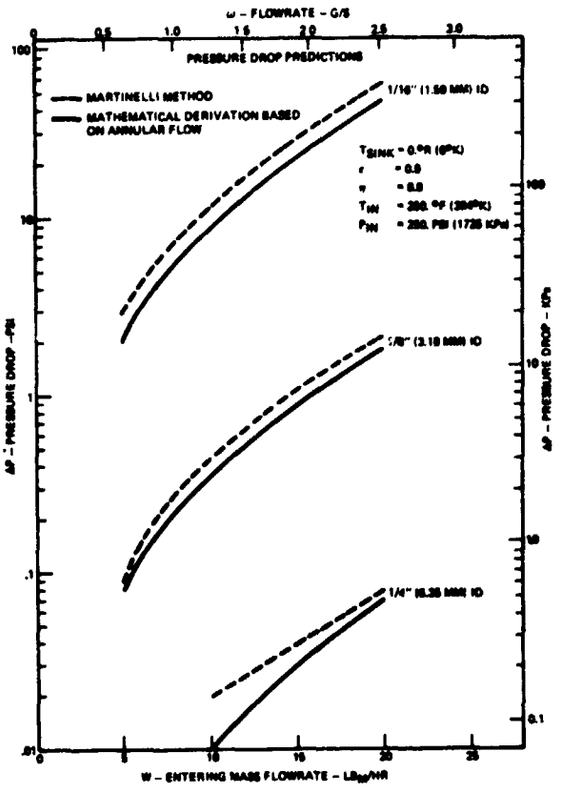

Fig. 22 Condenser pressure drop versus flowrate

References

1 Ginwala, K., "Engineering Study of Vapor Cycle Cooling Equipment for Zero-Gravity Environment," Wright Air Development Division Technical Report 60-776, Jan. 1961.

2 Dietz, J. B., et al., "Modulaur Radiator System Development for Shuttle and Advanced Spacecraft," ASME Paper No. 72-ENAv-34, presented at the Environmental Control and Life Support Systems Conference, San Francisco, Calif., 14–16 Aug. 1972.

3 Tufte, R. J., "Wide Heat Load Range Space Radiator Development," First Intersociety EC/LSS Conference, ASME Paper No. 71-Av-5, July 1971.

4 "Comparative Refrigerant Performance Rating," DuPont Freon Technical Bulletin RT-27, 1966.

5 Ostrach, S., and Koestel, A., "Film Instabilities in Two-Phase Flows," AICHE Paper No. 45, 6th National Heat Transfer Conference, Boston, Mass., 1963.

6 Soliman, M., and Berenson, P. J., "Flow Stability and Gravitational Effects in Condenser Tubes," the Fourth Int'l Heat Transfer Conference, Paris, France, 1970.

7 Kordyban, E. S., and Ranov, T., "Mechanism of Slug Formation in Horisontal Two-Phase Flow," *Journal of Basic Engineering*, Trans. ASME, Dec. 1970, pp. 857–864.

8 Denington, R. J., "Space Radiator Study," ASD-TDR-61-697, (DDC No. AD-424-419), Oct. 1963.

9 Miles, J. W., "The Hydrodynamic Stability of a Thin Film of Liquid in Uniform Shearing Motion," *Journal Fluid Mechanics*, 8, 1960, pp. 593–610.

10 Baker, O., "Design of Pipe Line for the Simultaneous Flow of Oil and Gas," *The Oil and Gas Journal*, July 26, 1954.

11 Haberstrah, "The Annular-Slug Transition," *Two-Phase Gas-Liquid Flow*, Special Summer Program at MIT, 27 July–7 Aug. 1964.

12 Suo, M., "Two-Phase Flow in Capillary Tubes," *Two-Phase Gas-Liquid Flow*, Special Summer Program at MIT, 27 July–7 Aug. 1964.

13 Suo, M., and Griffith, P., "Two-Phase Flow in Capillary Tubes," *Journal of Basic Engineering*, Trans. ASME, Series D, Vol. 86, No. 3, Sept. 1964, p. 577.

14 Martinelli, R. C., et al., "Isothermal Pressure Drop for Two Phase Flow in a Horisontal Pipe," Trans. ASME, Feb. 1944, pp. 139–151.

15 Griffith, D., "Two-Phase Flow in Pipes," *Advances in Heat Transfer*, MIT Press, 1963, p. 261–291.

16 Feldmanis, C., "Performance of Boiling and Condensing Equipment Under Simulated Outer Space Conditions," ASD-TDR-63-862, Wright-Patterson AFB, Nov. 1963.

17 Holden, P. C., and Stump, F. C., "Optimised Condenser-Radiator for Space Applications," ASME Paper No. 60-Av-16, Aviation Conference, Dallas, Texas 5–9 June 1960.

19 Akers, W. W., and Rosson, H. F., "Condensation Inside a Horizontal Tube," *Chemical Eng Prog Symposium*, Series 30, Vol. 56, p. 145–149.

20 Davis, E. J., and David, M. M., "Two-Phase Gas-Liquid Convection Heat Transfer," *I&EC Fundamental*, Vol. 3, No. 2, May 1964, pp. 111–117.

21 Namkoong, D., Block, H. B., and Macorko, R. P., "Photographic Study of Condensing Mercury Flow in 0 and 1-G Environments," NASA TN D-4023, June 1967.

22 Albers, J. A., and Macosko, R. P., "Experimental Pressure-Drop Investigation of Non-Wetting, Condensing Flow of Mercury Vapor In a Constant-Diameter Tube in 1-G and Zero-Gravity Environments," NASA TN D-2838, June 1965.

23 Albers, J. A., and Macosko, R. P., "Condensation Pressure Drop of Non-Wetting Mercury in a Uniformly Tapered Tube in 1-G and Zero-Gravity Environments," NASA TN D-3185, Jan. 1966.

APPENDIX B

A PHOTOGRAPHIC STUDY OF FLOW CONDENSATION IN 1G AND ZERO-G ENVIRONMENTS

Cs 1.5

A PHOTOGRAPHIC STUDY OF FLOW CONDENSATION IN 1-G AND ZERO-GRAVITY ENVIRONMENTS

Edward G. Keshock
Old Dominion University, Norfolk, Va., U.S.A.
Gordon Spencer
Burrell L. French
Johnson Space Center, NASA, Houston, Texas, U.S.A.
James L. Williams
Vought Systems Div., Dallas, Texas, U.S.A.

Abstract

High-speed photographs were taken of the flow condensation of refrigerant-12 in small diameter quartz tubes (3 mm). Photographs obtained under 1-g conditions permitted comparison of the flow regimes with the Baker chart predictions. Qualitative comparisons with other photographs taken under zero-g conditions appear to indicate no significant reduction of heat transfer under zero-g conditions.

INTRODUCTION

The present study[1] was undertaken as part of a broader program to develop a hybrid spacecraft heat rejection system, i.e. one in which the radiator could function either (1) conventionally with single-phase liquid flow through the radiator tubes or (2) as a condenser in a vapor compression refrigeration cycle, capable of accomodating two-phase condensing flow. The impetus for the development of such a hybrid system originates principally from the trend toward internal power requirements of space vehicles growing at a faster rate than the surface availability of space radiators. Feasibility studies[2] indicated that a vapor-compression refrigeration system could reduce radiator surface requirements significantly in some applications.

While unique developmental and system operational problems are associated with the successful operation of such a hybrid system [1], additional possible problems related to two-phase condensing flow processes (within the radiator/condenser (r/c) panel) in a zero-gravity environment must also be accurately evaluated and predicted. The broad objectives of the present study were (1) to experimentally determine operating characteristics of a full-scale multi-channel radiator/condenser panel, with refrigerant-12 (R-12) as the working fluid, in 1- and 0-g environments, (2) to establish and/or modify parameters and correlations capable of predicting heat transfer, pressure drop, and stability characteristics of such systems in 0-g environments.

In order to help achieve these objectives photographs of the two-phase flow condensation phenomena occurring in the condenser tubes under both 1- and 0-g conditions were desired. This information was obtained by high speed photographs of R-12 condensing in a system of three quartz tubes connected in parallel and modelled thermally and hydrodynamically after the r/c panel.

The present paper concerns itself primarily with the photographic measurement and analysis of condensation phenomena in a 1-g field. Also, some qualitative comparisons are made with photographs taken in 0-g. Quantitative comparisons with 0-g behavior are to follow as more 0-g photographic data become available.

If it is essential to predict flow regimes, so that heat transfer, pressure drop and stability characteristics may be more accurately predicted, it must first be determined whether existing flow regime maps, such as the Baker chart [2], accurately portray the flow regimes occurring in the given system over the range of operating conditions. Flow regime maps are available in the literature for both horizontal and vertical flows [2-3]. Generally these maps have been developed for boiling systems or for two-phase, two-component systems (e.g. air-water), which have often been obtained in rather large diameter systems. Whether or not the flow regimes predicted by such maps have any validity under 0-g conditions should be established by the present tests. Appropriate modifications to such maps, together with the related predictions of system performance, may be required.

PREVIOUS ZERO-G INVESTIGATIONS

One of the earliest investigations of condensing processes in zero-gravity conditions was conducted by Feldmanis [4], who made temperature, pressure, and photographic measurements of forced convection condensation of distilled water in a single, tapered, tube, with a 1.74 cm inlet i.d. He reported an increase in condensate temperature during low gravity conditions that may have been caused by reduced condensation heat transfer coefficients, possibly attributable to the absence of gravity forces acting to remove the condensate film from the cooled surface within the tube.

Two studies of significance, investigating the flow condensation of a non-wetting fluid (mercury) in tubes, were conducted by Albers and Macosko [5] and Namkoong, et al. [6]; both studies employed a Navy AJ-2 bomber flying a Keplerian trajectory to attain the 0-g environment. Tube sizes ranged from 0.686 to 1.245 cm i.d. Namkoong, et al. [6] reported a concentration of drops on the tube bottom and a shallow sloping interface under 1-g conditions, while in a 0-g environment the drops were uniformly distributed and the interface was vertical. Albers and Macosko reported that (1) measured overall static pressure drops at two mass flow rates were essentially the same for 1- and 0-g conditions, and

(2) the Lockhart-Martinelli parameter ϕ_g and the two-phase flow pressure gradient were affected negligibly by gravity, as also were the fog-flow correlations.

In the study related most closely to the present one, Soliman and Berenson [7] studied flow condensation of Freon-113 in a transparent multi-tube condenser. Both tapered and constant-diameter tubes were studied, the latter containing twisted tape and wire in some cases. Tube diameters ranged from 0.335 to 0.595 cm i.d. The gravitational effects studied, however, were those attained from operating the condenser in positions ranging from a +90-degree position (condensing downwards) to a -90-degree position (condensing upwards).

EXPERIMENTAL EQUIPMENT

Three test articles were fabricated--two full-scale radiator/condenser (r/c) panels, (Figure 1) and a system of three parallel-connected fused quartz tubes (Figure 2) modelled thermally and hydrodynamically after r/c panel number 2. The r/c panel number 2 was intended to provide quantitative engineering data in 1- and 0-g conditions, while the transparent quartz-tube fixture was intended to permit high-speed photographic analysis of the two-phase condensation phenomena, also under 1- and 0-g conditions. Testing was performed initially on the ground, with both horizontal and inclined flow passage orientations, and additionally in an aircraft flying 0-g trajectories.

The transparent quartz tube system is shown in the system schematic, Figure 3. The condensing fluid, R-12, is stored in a 75.7 liter tank that can be heated to provide the desired system operating pressure (0.0984 to 0.246 kgf/mm^2) by an immersion-

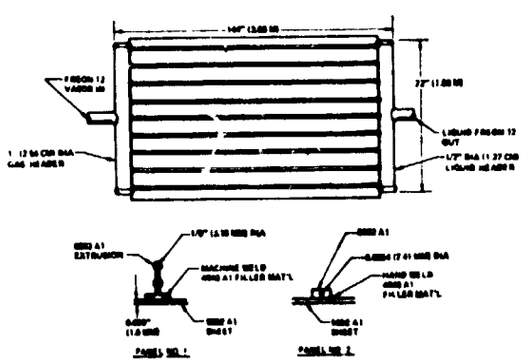

Fig. 1 RADIATOR/CONDENSER PANEL DESIGN

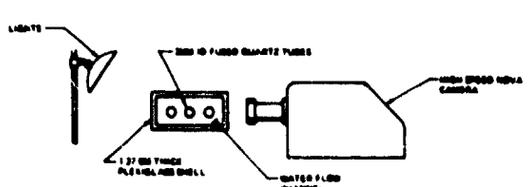

Fig. 2 FLOW VISUALIZATION APPARATUS

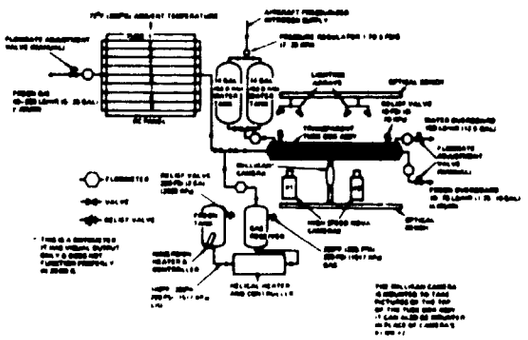

Fig. 3 TEST APPARATUS FLOW SCHEMATIC

type heater. The liquid R-12 withdrawn from the tank bottom passes through an electrical heating system where the R-12 is superheated to the desired degree. The heater is designed with a tortuous pathway system so that centrifugal forces maintain the liquid refrigerant in contact with the heater walls during weightless intervals. The R-12 then flows to a gas receiver so that any pressure fluctuations caused by flashing in the boiler may be damped out.

The superheated R-12 vapor flow is then directed to either the r/c panel or to the transparent tube fixture. In either case the exiting liquid R-12 passes through a flow metering valve which maintains the flowrate at the desired level 2.3-9.1 kgm/hr. The condensed R-12 is then either dumped overboard or to the atmosphere, depending upon whether flight tests (0-g) or ground tests are being conducted.

The quartz tube fixture is cooled by water (Figures 2, 3) stored in two 53-liter tanks in a closed loop parallel flow system (though in some initial tests an open coolant system was employed). The water temperature in the tanks ranged from 15.6-26.7°C, while the nominal flowrate was 45.4 kgm(m)/hr. The maximum temperature rise of the water was 17°C. The inlet R-12 temperature ranged from 47.2 to 86.7°C while pressures ranged from 0.110 to 0.179 kgf/mm^2.

Instrumentation on the transparent tube fixture consisted of inlet and outlet temperatures (immersion thermocouples) and pressures of the R-12, together with ΔP measurements across the quartz tube assembly. The inlet and exit temperature of the water system were also monitored by immersion thermocouples. Four surface temperature measurements of the plexiglas flow channel were also made. Flowrate measurements of both systems were made with turbine flow meters, while a rotameter was employed in the water system for 1-g tests.

The photographic observations were made with two high speed cameras (operated at 2000-7000 frames/second) and a low speed camera (400 frames/second). The low speed camera was mounted so as to view all three tubes from above, permitting observation phenomena within the parallel system. All three cameras were mounted on optical benches that permitted rapid repositioning along the length of the tubes. The high speed cameras viewed the transparent fixture from the side, as shown in Figures 2 and 4.

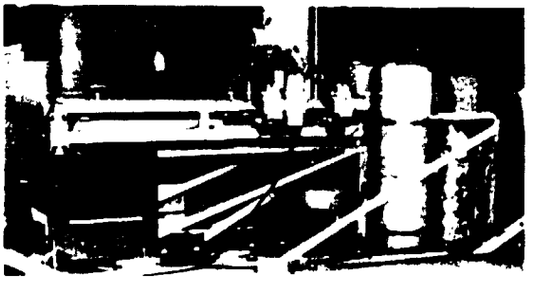

Fig. 4 EXPERIMENTAL TESTING ASSEMBLY

RESULTS

The types of flow regimes observed are shown schematically in Figure 5. This figure has been

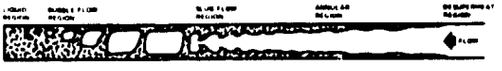

Fig. 5 SCHEMATIC OF CHARACTERISTIC FLOW REGIMES

developed after examination of numerous high-speed photographs taken at periodic intervals along the condenser tube's length. The tube inside diameter upon which these results are based was 2.62 mm. Flow rates of the condensing R-12 ranged from 2.3 to 9.1 kgm/hr, corresponding to G values of 42.2 to 168.9 x 10^3 kgm/m^2-hr. Inlet temperatures varied from several degrees superheat in some cases to saturation temperatures. Over the range of variables investigated no substantial differences were observed in the qualitative illustration of flow patterns depicted in Figure 6.

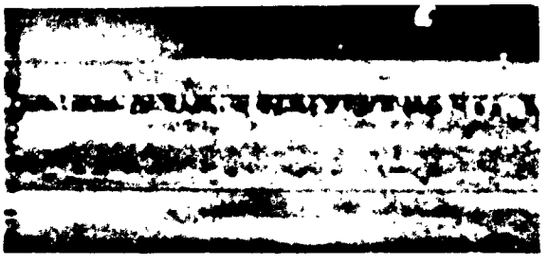

Fig. 6 CHARACTERISTIC FLOW PATTERNS-
(a) ANNULAR FLOW

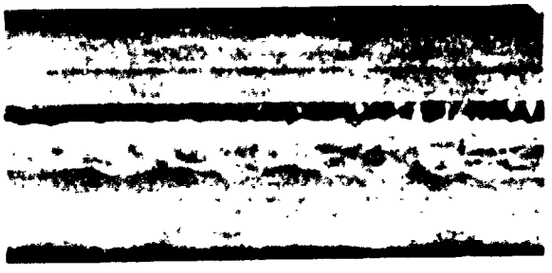

Fig. 6 (b) ANNULAR-STRATIFIED FLOW

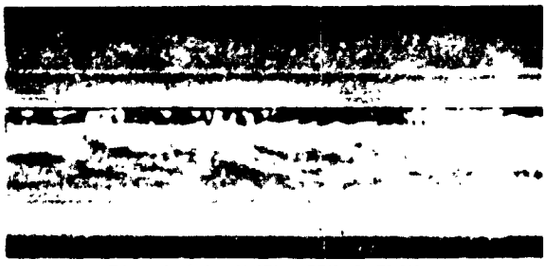

Fig. 6 (c) WAVY-ANNULAR FLOW

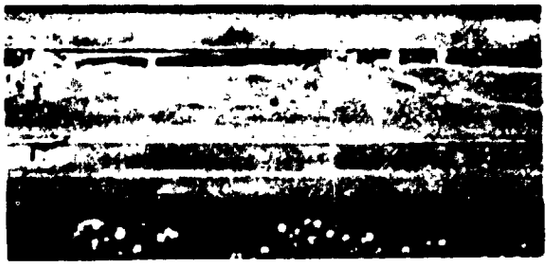

Fig. 6 (d) SLUG FLOW

Fig. 6 (e) ELONGATED BUBBLY FLOW

Fig. 6 (f) ISOLATED BUBBLE FLOW

Figure 6 consists of photographs of the condensation processes occurring under the conditions of a nominal system pressure of 230 psia. Shown in sequence are (a) ripply annular flow, with the liquid film distributed essentially uniformly along the tube wall, (b) annular-stratified flow, with a preponderance of the liquid flow along the tube bottom due to gravitational action, (c) wavy annular flow, in which the shearing action of the higher speed vapor flow initiates the growth of large amplitude waves, occasionally reaching the top of the tube, (d) slug flow, in which the regular and periodic bridging of the tube diameter

results in separated slugs of vapor moving above the liquid, (e) elongated bubbly flow, where the isolated vapor pockets have become more regularly shaped and widely spaced, and (f) isolated bubble flow, in which rather small vapor bubbles move along the top of the tube to complete extinguishment.

Evidence of the lack of distinct boundaries between various flow regimes is shown in Figure 7. Each of

Fig. 7 VARIETY OF FLOW PATTERNS AT IDENTICAL TEST CONDITIONS- (a) ANNULAR-STRATIFIED FLOW

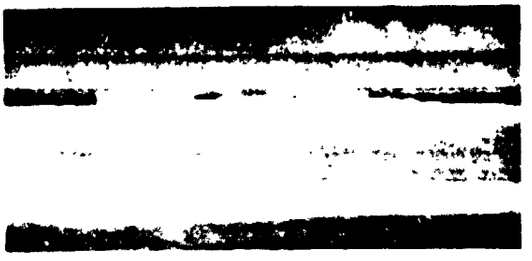

Fig. 7 (b) WAVY-ANNULAR FLOW

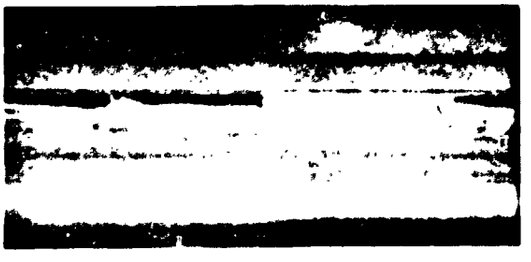

the photographs in Figure 7 was taken from the same roll of film, which represents less than one second of viewing the condensation process. The regimes observed at this particular location are (a) annular-stratified flow, (b) same as (a), but with complete, but intermittent, bridging of the tube diameter by the waves, (c) slug flow, in which distinct separation of vapor slugs by a continuous liquid column is evident.

The flow regimes observed are compared with those predicted by the Baker chart [2] in Figure 8. The coordinates of Figure 8 are functions of liquid and vapor mass flowrate and fluid properties [2,8] (viscosity, surface tension, density). The flow regimes were categorized into four groups: annular, annular-stratified, slug, and bubbly (ranges from

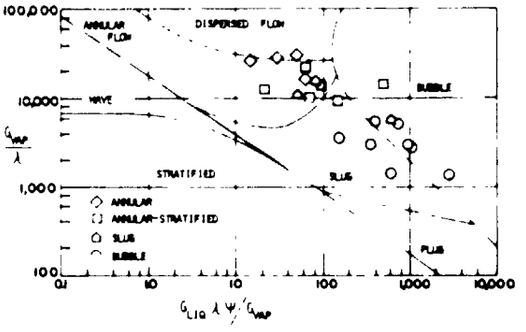

Fig. 8 BAKER CHART [2]

long elongated bubbles to small isolated bubbles).

Other qualitative results observed primarily in connection with differences between 1-g and 0-g flow patterns are as follows. As one would expect in the absence of gravitational forces, the condensate film in the annular region was uniformly distributed about the tube wall. It would be expected that the annular regime would persist over a longer distance in a 0-g environment. Verification of this expectation and mapping of the complete flow regimes in a 0-g environment is to be conducted as data from future 0-g flights become available.

Also, as one would expect, it was observed that in the bubble flow region the bubbles moved very nearly along the tube center, showing no affinity for the tube wall. From an overall standpoint, it appeared that there was little difference in heat transfer characteristics due to 0-g operation since there was no substantial changes in the point of complete vapor extinguishment for the same flow parameters.

A final qualitative difference between 1-g and 0-g flow conditions was the notably less irregular, less wavy character of the flow phenomena under 0-g conditions. In the annular regime the liquid film appeared significantly less wavy. Also, in a 1-g environment in the annular region, high-velocity disturbances appeared to disrupt the liquid film appreciably at regular intervals; under 0-g conditions the periodic high-velocity disturbances also persisted, but appeared to disrupt or distort the annular film to a much smaller degree.

DISCUSSION OF RESULTS

The flow regimes observed, illustrated in Figures 5 and 6, differ substantially from the descriptions of condensing horizontal flows in tubes presented in [4-6,8]. Also, as generally described in the literature wetting fluids generally form a thin annular layer at the heat transfer surface, from which layer drops are sometimes broken off and entrained in the vapor core, resulting in mist-annular flow. Very little droplet entrainment was evident in the present study, perhaps because of relatively low vapor velocities.

Analytical models of condensation in tubes often consider the annular flow regime to persist

throughout the tube length, based upon the supposition that annular flow is indeed the dominant flow regime. The present results indicate annular flow to exist over only roughly half of the condensing region, after which the slug flow and bubble flow regimes exist.

In a study of wetting and non-wetting mercury condensation [8] fluoroscopic observations indicated a fog-flow regime terminated by a rather elongated sloping interface at the "point" of complete condensation. Their observation of the non-wetting flow indicated a predominantly fog-flow regime with some droplets at the walls, terminated by a more or less vertical, distinct interface (see also [5,6]). These observations led to their employment of a fog-flow model for predicting pressure drop. As seen from Figure 6, not only does a fog-flow regime not exist, but neither does a distinct liquid-vapor interface at the point of complete condensation exist; but rather, elongated vapor bubbles gradually become smaller until they eventually disappear.

Concerning settling of liquid along the tube bottom as in Figure 6 (b), (c), this regime might be considered a combination of stratified and annular flow. Regarding heat transfer in this region, certainly the accumulation of liquid along the tube bottom diminishes the rate of heat transfer, but at the same time, continuous draining of the liquid from the top half of the tube promotes heat transfer in that region. Contrasting this picture with that existing in 0-g, the essentially uniform film thickness existing in 0-g may have a uniformly good heat transfer rate along the tube periphery that may be equivalent to the "average" heat transfer conditions existing in 1-g, described in the previous sentence. Perhaps this accounts for the observation that no substantial difference in condensation length is discernible for 1-g and 0-g conditions for the same heat transfer and flow parameters. It should be noted that possible differences in the other flow regime also affecting the heat transfer characteristics have not been investigated due to unavailability of data. This will be the subject of future investigation.

The comparison of measured and predicted flow regimes shown in Figure 8 warrants some elaboration. The Baker chart is well in accord with physical reality in the annular flow region, where at the higher system flow rates motion picture photographs did give some evidence of the existence of dispersed flow. However, the stratified-annular flow regime observed has no counterpart in the Baker categorization. If the stratified-annular regime may be classified simply as a special case of annular flow, then the Baker chart is in reasonable accord with reality.

The only three observations of a slug-flow regime fall just outside of the slug-flow boundaries. This is not unusual in that the flow regime boundaries must be realistically considered to be somewhat "blurred", rather than discrete. The preponderance of bubbly-flow data points are seen to fall along the slug-bubble boundary or slightly within the bubbly regime. In general, the Baker chart predictions appear reasonably good.

CONCLUSIONS

The principal conclusions of the present study are: (1) the Baker chart predicts the condensing flow regimes reasonably well; and (2) condensation heat transfer is not appreciably affected by a 0-g environment for the system described.

FOOTNOTES

* Conducted under NASA contract NAS9-13410.

** Conducted by Vought Missiles and Space Division, LTV, Dallas, Texas, under the auspices of the Johnson Space Center, Houston, Texas.

REFERENCES

[1] Williams, J. L., Keshock, E. G. and C. L. Wiggins: "Development of a Direct Condensing Radiator for Use in a Spacecraft Vapor Compression Refrigeration System". ASME Jnl. of Eng. for Industry (1973)

[2] Baker, O.: "Design of Pipe Line for the Simultaneous Flow of Oil and Gas". The Oil and Gas Journal (July 26 1954)

[3] Baker, James L.: "Flow-Regime Transitions at Elevated Pressures in Vertical Two-Phase Flow". ANL-7093 (Sept. 1965)

[4] Feldmanis, C.: "Performance of Boiling and Condensing Equipment Under Simulated Outer Space Conditions". ASD-TDR-63-862, Wright-Patterson AFB (Nov. 1963)

[5] Albers, J. A. and R. P. Macosko: "Experimental Pressure-Drop Investigation of Non-Wetting, Condensing Flow of Mercury Vapor in a Constant Diameter Tube in 1-g and Zero-Gravity Environments". NASA TN D-2828 (June 1965)

[6] Namkoong, D. et al.: "Photographic Study of Condensing Mercury Flow in 0 and 1-g Environments". NASA TN D-4023 (June 1967)

[7] Soliman, M. and P. J. Berenson: "Flow Stability and Gravitational Effects in Condenser Tubes". Proc. Int. Ht. Tr. Conf., Paris (1969)

[8] Koestel, A., et al.: "Study of Wetting and Non-Wetting Mercury Condensing Pressure Drops". NASA TN D-2514 (Nov. 1964)